Comparison of Reaction in Catalyst Pellet Between Three-Dimensional Computational Fluid Dynamics and One-Dimensional Multiphysics Simulations

A Major Qualifying Project Report Submitted to the Faculty of
Worcester Polytechnic Institute in partial fulfillment of the requirements for the
Degree of Bachelor of Science

Submitted by:

Christian P. Waller
April 2010

Approved by:

Dr. Anthony G. Dixon, Advisor

EXECUTIVE SUMMARY

The field of computational fluid dynamics (CFD) was developed with the advent of powerful computing hardware in the mid-twentieth century. Computational fluid dynamics revolutionized research into fluid dynamics because of its ability to numerically solve difficult systems of equations. As commercially available CFD code evolved the number of industries which found use for such an application also grew. Recently the field of chemical reaction engineering has applied CFD to the difficult problems of characterizing heat, mass transfer, and fluid flow effects on chemical systems.

This study investigates the kinetics of the esterification of methanol and acetic acid into methyl acetate and water so that this reaction can be simulated using CFD. Fluent, a popular CFD package, was used to simulate the esterification reaction in a β-zeolite catalyst pellet using a three-dimensional (3D) model. The reaction and diffusion limitations of the system are characterized by examining the effects of various aspects of the pellet geometry, such as edges and holes. The distribution of products throughout the pellet is shown to qualitatively agree with data obtained from H-NMR analysis with a fair degree of accuracy.

Due to a lack of experimental data to validate the model, this study focuses instead on approximating the complex 3D geometry by a simpler 1D system modeled in the multiphysics software COMSOL. In particular, the relationship between catalyst surface area, catalyst volume, and overall reaction rate is examined. The results of the 3D and 1D simulations demonstrate that a properly defined 1D system can accurately model some aspects of a 3D system – for example, the internal concentration profile was approximated by the 1D model very well, but the overall reaction rate was significantly different from that given by the 3D model. Several suggestions are made on how this project can be expanded and improved upon in the future.

ACKNOWLEDGEMENTS

The work presented in the report is the direct result of the contributions of several individuals who helped guide me throughout this process. Without the influence and mentoring of these people I would not have been able to accomplish as much as I have.

First and foremost I would like to extend my sincere gratitude to Professor A. G. Dixon for his continual academic and moral support throughout the entirety of this process. Professor Dixon's experience with conducting academic research and expertise in the field of computational fluid dynamics have both proved to be invaluable resources.

I also owe a great deal of gratitude to the members of the steam reforming group at the Chilton site of Johnson Matthey in Billingham, UK. Specifically I would like to acknowledge Dr. Michiel Nijemeisland and Dr. E. Hugh. Stitt. The guidance which I was lucky enough to receive during my first foray into the world of industrial chemical engineering opened my eyes to the opportunities which await me after graduation. Both Dr. Nijemisland and Dr. Stitt served as excellent role models and examples of true professionals. Thank you for making this project possible.

TABLE OF CONTENTS

CHAPTER 1

Introduction

The chemical process industry, which employs more than one million individuals and generates more than $400 billion per annum in the United States alone, produces the materials which make nearly every commercially available product. Catalysts play an integral role in this industry by facilitating a wide range of chemical processes including steam reforming, ammonia synthesis, methanol synthesis, hydrocracking, and hydrodealkylation. Over 70% of industrial processes utilize catalysts, accounting for over 90% by volume of chemical products (Catalytic Processes and Materials, 2011). Proper catalyst design requires one to consider a wide range of design variables, such as particle geometry, size, and diffusion characteristics (Sie & Kirshna, 1998). A thorough understanding of the mechanisms of transport and reaction within catalysts allows for improvements upon the design of existing catalysts, thereby increasing the economic incentive of processes.

The foundations of modern research into the diffusion and reaction phenomena of catalysis were laid in the seventeenth century with the birth of experimental fluid dynamics. Early experiments provided empirical data on fluid flow, such as the relationship between drag and the square of velocity. Towards the end of the seventeenth century the theoretical framework of fluid dynamics began to take form, beginning with the theoretical derivation of the velocity-squared law from the laws presented in Newton's *Principia*. Advancements in the realm of theoretical fluid dynamics continued throughout the eighteenth and nineteenth centuries via the research of Bernoulli, Pitot, Euler, Navier, Stokes, and others.

Research in all fields of engineering and science existed in two worlds, pure theory and pure experiment, until the advent of computers in the 1960s. The raw computational power of computers coupled with numerical algorithms which describe fluid flow, diffusion, and reaction provided researchers with a tool to numerically solve systems of equations which would be difficult or impossible to solve

otherwise. Additionally, the ability to numerically simulate fluid dynamics and reaction allowed scientists to investigate phenomena in locations which are inaccessible in the laboratory due to limitations in experimentation technology. For example in systems which operate at a high temperature or pressure (e.g. steam methane reforming) or are highly corrosive the extreme conditions preclude gathering data via physical experimentation, thereby rendering simulation as the only method of data acquisition.

As computing technology matured and more powerful processors were developed, increasingly complex simulations could be solved. While early simulations of diffusion and reaction investigated catalysis in one particle in one dimension (1D), modern simulations often model tens, if not hundreds, of particles in three dimensions (Nijemeisland & Dixon, 2001). The advantages offered by 3D simulations over 1D simulations (namely a closer approximation of reality) are counterbalanced by the drawbacks introduced by the dramatic increase in the complexity of the system – namely an increase in the time and computational power needed to solve the simulation. Because any given chemical process can operate under a range of conditions, simulating every set of operating conditions requires a significant investment of time and capital. Therefore, it is desirable to reduce a complex 3D model to a simpler 1D or 2D model whenever it is possible to do so without sacrificing the quality of the simulation results.

1.1. Problem Statement

The present study investigates diffusion and reaction within a 3D catalyst pellet. compares diffusion and reaction in 3D computational fluid dynamics simulations to diffusion and reaction in 1D multiphysics simulations. The reaction of interest is the forward reaction of the esterification of methanol and acetic acid into methyl acetate and water over a β-zeolite catalyst (the reverse reaction and dimerization reaction of methyl acetate into dimethyl acetate are not considered), which is given by:

$$CH_3OH + CH_3COOH \xrightarrow[\beta-zeolite]{} CH_3COOCH_3 + H_2$$

The original intent of the work was to compare the results of 3D CFD simulations to experimental H-NMR data of reaction over a catalyst pellet. Magnetic resonance imaging (specifically H-NMR imaging) has been recognized as a powerful tool to noninvasively investigate diffusion and reaction inside

of a catalyst particle in situ (Huang, Yijiao, Reddy Marthala, Wang, Sulikowski, & Hunger, 2007). Unfortunately the H-NMR experiments failed to produce any quantitative results due to a lack of chemical resolution for the chosen system – the only data of significance shows a qualitative distribution of methanol within the pellet. Therefore the focus of the project shifted to comparing the results of diffusion and reaction in 3D computational fluid dynamics simulations to 1D multiphysics simulations in order to determine whether a 1D approximation of a 3D geometry can provide accurate results.

The 3D system geometry was generated using GAMBIT 2.4.6, a computer aided design program. The CFD simulations were completed in Fluent 6.3.26 in 3D using the finite volume spatial discretization method. The multiphysics simulations were completed in COMSOL 3.5a using the Mass Transport application in the Chemical Engineering Module in 1D using a finite element scheme.

Both the 1D and 3D simulations required information about the kinetics and diffusion of the system. In order to supply the former, a kinetic experiment was designed and carried out to determine the temperature dependence of the rate constant of the reaction. The diffusion parameters for species transport were calculated using the Wilke-Chang equation.

CHAPTER 2

Background

2.1. Cation Exchange Polymers

Solid catalysts are widely used in the chemical process industry to facilitate a number of chemical processes (e.g. steam reforming, ammonia synthesis, alcohol synthesis). One reason heterogeneous catalysts are widely used is that they offer several economic advantages compared to their homogeneous counterparts. Some of these advantages include ease of product separation from catalyst material, less potential for contamination, and reduced potential for equipment corrosion (Harmer & Sun, 2001).

Cation exchange polymers are one class of heterogeneous catalysts. Ion exchange polymers are insoluble in and can exchange ions (existing within its pores) with a fluid passing through it. One category of cation exchange catalysts are known as zeolites. Zeolites are crystalline aluminosilicates whose three-dimensional structures boast the unique property of uniform pore sizes (Maesen, 2007, p. 1). The crystal structure of zeolites (see Figure 1) consists primarily of SiO_2, but at certain sites the silicon has been replaced by aluminum. A charge imbalance is introduced at sites where Al^{3+} replaces Si^{4+} and gives the crystal a net negative charge which allows various cations (e.g. Na^{+}, K^{+}, Ca^{2+} etc.) to enter its pores.

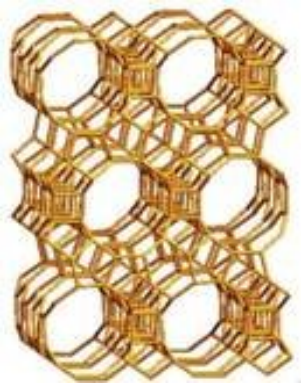

FIGURE 1: B-ZEOLITE CRYSTAL STRUCTURE

Zeolites, whose pores measure on the molecular scale, are commonly used as molecular sieves which selectively allow diffusion of molecules which are small enough to fit inside its pores. This property of zeolites makes them an attractive option when a high degree of selectivity is required, as in the case for the formation of xylene from toluene and methane (Fogler, 2006). In this reaction methane and toluene diffuse into the zeolite and react

to form a mixture of ortho, meta, and para xylenes. Due to the size of the pores only para-xylene is able to diffuse out of the zeolite, while ortho- and meta-xylene react on interior active sites to isomerize into para-xylene. Although molecules are constantly diffusing into and out of the zeolite, the crystal typically retains its original structure with no appreciable changes in size or conformation (Dyer, 2007, p. 532).

The catalyst used in this study was β-zeolite, a large-pored zeolite which is used in processes such as catalytic cracking, isomerization, alkylation, and disproportionation (Su & Norberg, 1997). This catalyst is a solid acid catalyst which offers the functionality of an acid to facilitate the esterification reaction on a solid matrix, allowing for easy separation of products from the catalyst.

2.2. Heterogeneous Catalysis

Heterogeneous catalysis typically occurs at the interface between two or more phases. For the esterification reaction considered in this study, the fluid mixture consisting primarily of methanol and ethanol constitutes the first phase and the zeolite catalyst is the second phase. Because the catalytic reaction occurs at the interface between phases, catalysts are typically designed to maximize surface area without compromising necessary mechanical properties of the catalyst structure. The most common method of maximizing the surface of a catalyst is to introduce an internal porous structure. Typical silica-alumina cracking catalysts have pore volumes of 0.6 cm^3/g and pore radii of 4 nm, resulting in surface areas of 300 m^2/g (Fogler, 2006).

In contrast to porous catalysts where the active material is part of the support structure, supported catalysts have the active material dispersed over the surface of a less active substrate which provides the catalyst structure. Supported catalysts are an attractive option when the active material is very expensive, as is the case with pure metals or metal alloys. A third category of catalysts is monolithic catalysts. These catalysts offer such high activity that they do not require a porous structure to achieve high reaction rates. These catalysts are typically used in reactions where pressure drop and heat removal are major concerns, such as the catalytic conversion of combustion engine exhaust gases (Fogler, 2006).

2.2.1. Steps in a Heterogeneous Catalytic Reaction

The first step in a heterogeneous catalytic reaction involves mass transfer from the bulk fluid to the external catalyst surface. In order to reach the catalyst surface, reactants must diffuse through a boundary layer which surrounds the catalyst pellet. The rate of mass transfer for a reactant A at bulk concentration C_{Ab} diffusing through a mass transfer boundary layer is given by

$$\text{Rate} = k_c(C_{Ab} - C_{As})$$

where k_c is the mass transfer coefficient which accounts for the resistance to mass transfer resulting from the boundary layer and C_{As} is the concentration of A at the external catalyst surface. Further discussion of the mass transfer coefficient and effects of external diffusion follow in Section 2.2.2.

After reaching the external surface of the catalyst, reactant A must diffuse from the external surface through the pore network of the pellet. While diffusing through the pore network, reactant A encounters active catalyst sites along the pellet walls and reacts. Whether or not internal diffusion limits the overall rate of reaction is dependent upon pellet size (Fogler, 2006). In a large pellet it takes a long time for species to diffuse into and out of the pellet interior, thus reaction is limited to areas near the external surface of the pellet. For a small pellet, species readily diffuse into and out of the pellet and reaction occurs throughout the entire pore network.

When the reactant A encounters an active catalyst site, it must be adsorbed onto the catalyst surface. This process is represented by the reaction. The rate of adsorption of species A onto active sites is directly proportional to the concentration of A and the concentration of vacant sites. The rate at which A desorbs from active sites without reacting is generally a first order process which is directly proportional to the concentration of active sites occupied by A (Fogler, 2006). The rate of adsorption is nearly independent of temperature while the rate of desorption increases exponentially with increasing temperature (Fogler, 2006).

Once reactant A is adsorbed onto the active site the reaction can proceed in a number of different ways, such as via the Eley-Rideal reaction. Following reaction, the products must leave the active sites via desorption.

Both the transport (i.e. diffusion, adsorption, and desorption) steps and reaction steps contribute to the overall reaction rate of the system. If the diffusion steps are much slower than the reaction steps, the system is said to be diffusion limited. In such a system the reactant species are converted to products faster than new reactant species can diffuse to the active sites of the catalyst. In contrast, if the reaction occurs much slower than the diffusion of species from the bulk fluid to the external catalyst surface, the system is said to be reaction limited. Because the diffusion of molecules occurs much quicker than the reaction, the concentration of species in the bulk fluid and at active sites within the catalyst is constant (Fogler, 2006).

2.2.2. Importance of External Diffusion in Heterogeneous Reactions

External diffusion can play a major role in the overall reaction rate of a heterogeneous catalytic reaction. When a species diffuses into a catalyst pellet, it must pass through a mass transfer boundary layer which surrounds the catalyst pellet. The thickness of this boundary layer is defined as the distance from the surface of the solid to the point where the concentration of the diffusing species equals 99% of its bulk concentration (Fogler, 2006). This boundary decreases in thickness with increasing velocity. Therefore, because the mass transfer boundary layer effectively accounts for all of the resistance to mass transfer from the bulk fluid to the pellet, external diffusion can be neglected at high fluid velocities.

The simplest definition of the mass transfer coefficient is

$$k_c = \frac{D_{fluid}}{\partial} \qquad \textbf{EQUATION 1}$$

where D_{fluid} is the diffusivity of the fluid and ∂ is the thickness of the mass transfer boundary layer. However, it is difficult to experimentally determine the thickness of the boundary layer surrounding the pellet. Fortunately there exist a number of heat transfer correlations which are analogous to mass transfer correlations. As the one-dimensional simulation presented in this study used a spherical pellet model, the Frössling correlation (Equation 2) for flow around a single sphere is most appropriate.

$$Sh = 2 + 0.6Re^{1/2}Sc^{1/3} \qquad \textbf{EQUATION 2}$$

The Sherwood (Sh), Reynolds (Re), and Schmidt (Sc) numbers are given by

$$Sh = \frac{k_c d_p}{D_{fluid}} \qquad \textbf{EQUATION 3}$$

$$Re = \frac{\rho d v}{\mu} \qquad \textbf{EQUATION 4}$$

$$Sc = \frac{\mu}{\rho D_{fluid}} \qquad \textbf{EQUATION 5}$$

where d_p is the particle diameter, ρ is the fluid density, v is the fluid velocity, and μ is the dynamic viscosity of the fluid. The Frössling correlation shows that in order to increase the mass transfer coefficient one must either decrease the particle size or increase the fluid velocity.

2.3. Esterification Reaction Mechanism and Rate Models

2.3.1. Mechanism of Esterification of Acetic Acid and Methanol

The reaction of esterification of acetic acid and methanol is a well-studied reaction. The mechanism for this reaction over a solid acid catalyst proceeds by the following steps (Teo & Saha, 2004). In the first step a hydrogen atom from the acid catalyst protonates the acetic acid.

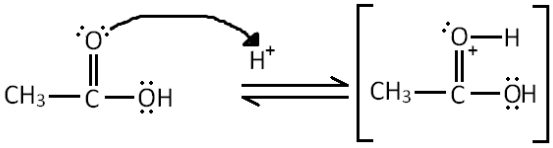

This protonation forms an unstable transition state which is stabilized when a pair of electrons leaves the π bond between carbon and oxygen and becomes a lone pair on the oxygen. This movement of electrons forms a primary carbocation which is then attacked by the nucleophile methanol.

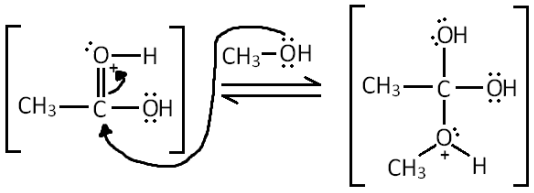

An unstable oxygen cation is formed once again, and the molecule quickly transfers hydrogen atom from the oxygen cation to a nearby oxygen where there is a region of greater electron density. The transfer of off of the oxygen cation creates a good leaving group and the molecule loses a molecule of water, creating a primary carbocation. To stabilize the molecule, the oxygen atom which is not bonded to the methyl group simultaneously donates a pair of electrons to form a π bond with the carbon atom.

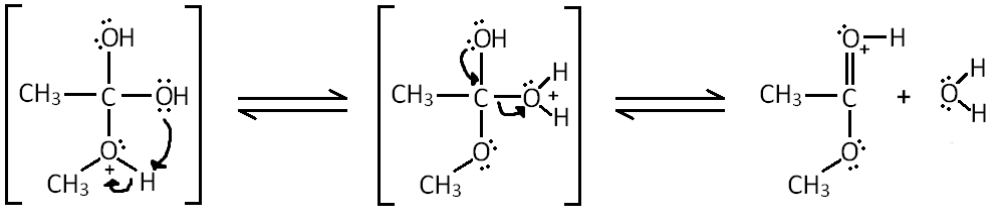

In the final step of the reaction the water molecule deprotonates the oxygen cation, resulting in the product methyl ester. The hydronium ion can serve both as a vehicle to regenerate the acid catalyst and as a Brønsted acid site.

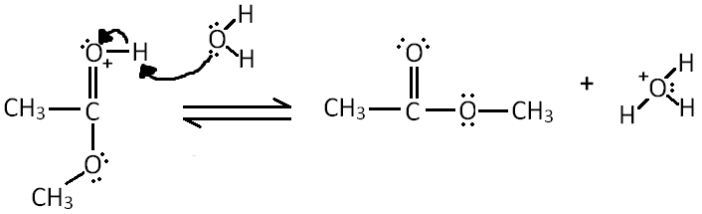

2.3.2. Pseudo-Homogeneous

In reactions which occur on the surface of a catalyst the reactants must first diffuse through the bulk solution onto the surface of the catalyst, then they must diffuse into the pores of the catalyst, and finally they must adsorb onto the active sites of the catalyst. The pseudo-homogeneous rate model offers a simplified rate expression by assuming that the adsorption of reactants onto the active sites of the catalyst is instantaneous. If one were to consider both the forward and reverse reactions of the esterification of acetic acid and methanol, one would write the pseudo-homogeneous rate model as

$$r_{methanol} = -\vec{k}\left(C_{methanol}C_{acetic\ acid} - \frac{1}{K}C_{methyl\ acetate}C_{water}\right) \quad \textbf{EQUATION 6}$$

where $K = \frac{\vec{k}}{\overleftarrow{k}}$, $\vec{k}$ is the forward rate constant, $\overleftarrow{k}$ is the reverse rate constant, and C_i is the concentration of species i. Because this study only investigates the forward reaction, the pseudo-homogenous rate model is written as

$$r_{methanol} = -kC_{methanol}C_{acetic\ acid} = r_{acetic\ acid} = -r_{methyl\ acetate} = -r_{water}$$

EQUATION 7

2.3.3. Water Inhibition on Cation Exchange Polymers

Diffusion, adsorption, and desorption play a significant role in the efficiency of heterogeneous catalysts. Although the reverse reaction contributes to slowing the production of product, studies show that when water is present as a product of reaction it inhibits the forward reaction much more than the reverse reaction (du Toit & Nicol, 2004, p. 219).

Take for example the esterification of an acid and alcohol over the cation exchange polymer Amberlyst®-15. Amberlyst®-15, shown in Figure 2, is a macroreticular copolymer of sulfonated polystyrene and divinylbenzene, which acts as a crosslinking agent for the polymer, increasing the crystallinity and strength of the polymer (Harmer & Sun, 2001). The hydrogen on the sulfur group of polystyrene is very acidic and readily protonates the acid to begin the mechanism outlined in Section 2.2. However, as water is produced it readily deprotonates the acid sites on the catalyst, reducing the number of available sites for catalytic reaction and slowing the reaction rate. Although hydronium ions can act as Brønsted acid sites, these sites are considerably less active than the acid sites on the catalyst (du Toit & Nicol, 2004, p. 221).

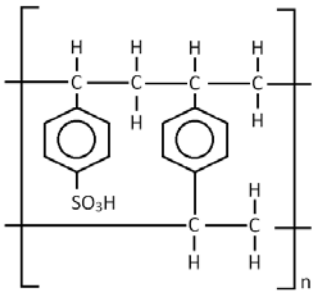

FIGURE 2: POLYSTYRENE-DIVINYLBENZENE

2.4. Historical Methods of Investigating Diffusion and Reaction in Heterogeneous Catalysis

The process of diffusion and reaction in commercial applications generally occurs in more than one spatial dimension. The costs associated with devising and conducting experiments into the behavior of diffusion and reaction in commercial processes make simulation an attractive option. Furthermore

experimentation offers little insight into the events occurring within heterogeneous catalysts, limited by current probe technology. Several different models, of varying complexity, are described in Sections 2.4.1 and 2.4.2.

2.4.1. Homogeneous Models

Early research in simulations of diffusion and reaction within heterogeneous catalysts was severely limited by the computing power available at the time, which precluded all but the simplest of catalyst geometries and diffusion-reaction mechanisms. Fixed bed reactors were among the first types of chemical reactors investigated due to their use in a variety of chemical processes. The earliest computational research of fixed bed reactors used homogeneous models which do not explicitly account for the presence of catalyst. The simplest of these models is one-dimensional and assumes that variations in concentration and temperature occurred only along the axial length of the rector. For this model, the conservation equations under steady state can be written as:

$$\rho_c r_A + u_s \frac{dC_A}{dz} = 0 \qquad \textbf{EQUATION 8}$$

$$u_s \rho_b c_p \frac{dT}{dz} - \rho_c(-\partial H) r_A + 4\frac{U}{d_t}(T - T_r) = 0 \qquad \textbf{EQUATION 9}$$

where u_s is the superficial fluid velocity, C_A is concentration of species A, z is the axial direction, ρ_c is the catalyst density, r_A is the rate of disappearance of reactant A, ρ_B is the bulk density, c_p is the heat capacity, ∂H is the heat of reaction, d_t is the tube diameter, T is temperature, and T_r is the reference temperature (Froment & Bischoff, 1979).

Although convenient to use and relatively untaxing on computational hardware, the one-dimensional homogeneous model does not account for any variations in flow profiles or the mixing behavior of the fluid which results from the presence of a solid catalyst. This limitation led to the development of a model which accounts for the mixing effects by introducing an effective diffusivity which accounts for the fluid flow around the solid particle.

Two-dimensional homogeneous models improve upon one-dimensional models by introducing variable gradients in the radial direction. This improvement is especially significant in simulations where

heat effects are especially important, as the fluid characteristics near the tube wall are significantly different than those in other regions (Froment & Bischoff, 1979). The conservation equations under steady-state conditions for a two-dimensional homogeneous model can be written as:

$$\varepsilon D_{er}\left(\frac{\partial^2 C_A}{\partial r^2}+\frac{1}{r}\frac{\partial C_A}{\partial r}\right)-u_s\frac{\partial C_A}{\partial z}-\rho_s r_A=0 \qquad \textbf{EQUATION 10}$$

$$k_{er}\left(\frac{\partial^2 T}{\partial r^2}+\frac{1}{r}\frac{\partial T}{\partial r}\right)-u_s\rho_b c_p\frac{\partial T}{\partial z}+\rho_c(-\partial H)r_A=0 \qquad \textbf{EQUATION 11}$$

where r is the radial direction, D_{er} is an effective radial diffusivity, and $k_{er}$is an effective thermal conductivity.

2.4.2. Heterogeneous Models

Heterogeneous models differ from homogeneous models in that they account for differences between the conditions in the fluid and conditions in the solid. Two sets of conservation equations, one for the fluid region and one for the solid region, must be written to describe diffusion and reaction in heterogeneous models. For the simplest one-dimensional heterogeneous model these equations can be written as:

Fluid

$$u_s\frac{dC}{dz}+k_c a_v(C_A-C_{As})=0 \qquad \textbf{EQUATION 12}$$

$$u_s\rho_b c_p\frac{dT}{dz}-h_f a_v(T_s-T)+4\frac{U}{d_t}(T-T_r)=0 \qquad \textbf{EQUATION 13}$$

Solid

$$\rho_c r_A=k_g a_v(C_A-C_{As}) \qquad \textbf{EQUATION 14}$$

$$h_f a_v(T_s-T)=\rho_c(-\partial H)r_A \qquad \textbf{EQUATION 15}$$

Boundary Conditions

$$C_A=C_{A0}\ \text{at}\ z=0$$

$$T=T_0\ \text{at}\ z=0$$

where a_v is the catalyst surface area per reactor volume, h_f is a heat transfer coefficient analogous to the mass transfer coefficient, and C_{As} and T_s are the concentration of A and the temperature on the surface of the solid (Froment & Bischoff, 1979).

When variations in the resistance to heat and mass transfer exist within the solid particle, the rate of reaction within the particle also varies. Therefore Equations 12 through 15 must be revised to incorporate the concentration and temperature gradients within the particle and are rewritten as:

Fluid

$$u_s \frac{dC}{dz} + k_c a_v (C_A - C_{As}) = 0 \qquad \textbf{EQUATION 16}$$

$$u_s \rho_b c_p \frac{dT}{dz} - h_f a_v (T_s - T) + 4\frac{U}{d_t}(T - T_r) = 0 \qquad \textbf{EQUATION 17}$$

Solid

$$\frac{D_e}{r^2}\frac{d}{dr}\left(r^2 \frac{dC_A}{dr}\right) - \rho_c r_A = 0 \qquad \textbf{EQUATION 18}$$

$$\frac{k_e}{r^2}\frac{d}{dr}\left(r^2 \frac{dT}{dr}\right) + \rho_c(-\partial H) r_A = 0 \qquad \textbf{EQUATION 19}$$

Boundary Conditions

$$C_A = C_{A0}, T = T_0 \text{ at } z = 0$$

$$\frac{dC_A}{dr} = \frac{dT}{dr} = 0 \text{ at } r = 0$$

$$-D_e\left(\frac{dC_A}{dr}\right) = k_c(C_{As} - C_A) \text{ at } r = r_o$$

$$-k_e\left(\frac{dT}{dr}\right) = h_f(T_s - T) \text{ at } r = r_o$$

where D_e and k_e are the effective diffusivity and effective thermal conductivity (Froment & Bischoff, 1979). The solid particle and fluid regions are divided into many small volumes, across the boundaries of which Equations 16 through 19 are solved. Because these equations are highly nonlinear they are typically solved numerically via an iterative process; however analytical solutions are possible for first-order irreversible reactions where the solid is isothermal (Froment & Bischoff, 1979).

Avci et. al (2001) used a 1D heterogeneous model to simulate hydrogen production from methane. The temperature profiles for the simulated steam reforming system closely approximated experimental values, but the simulated hydrogen and carbon monoxide yields positively deviated from experimental results. Furthermore the simulated methane conversion levels were lower than those reported in experimental data. The authors concluded that the simplified kinetics employed in the simulation caused these deviations and that a more accurate kinetic model could resolve these issues.

A two-dimensional heterogeneous model can be introduced to improve upon the one-dimensional heterogeneous models described above. The following mathematical model describes such a two-dimensional system:

$$\varepsilon D_{er}\left(\frac{\partial^2 C}{\partial r^2}+\frac{1}{r}\frac{\partial C}{\partial r}\right)-\mathrm{k_c a_v}(\mathrm{C_A}-\mathrm{C_{As}})-\mathrm{u_s}\frac{\partial \mathrm{C}}{\partial \mathrm{z}}=0 \qquad \textbf{EQUATION 20}$$

$$k_{er}^{f}\left(\frac{\partial^2 T}{\partial r^2}+\frac{1}{r}\frac{\partial T}{\partial r}\right)-h_f \mathrm{a_v}(\mathrm{T_s}-\mathrm{T})-\mathrm{u_s}\rho_\mathrm{b}\mathrm{c_p}\frac{\partial \mathrm{T}}{\partial \mathrm{z}}=0 \qquad \textbf{EQUATION 21}$$

$$\mathrm{k_c a_v}(\mathrm{C_A}-\mathrm{C_{As}})=\eta\rho_\mathrm{b}\mathrm{r_A} \qquad \textbf{EQUATION 22}$$

$$\mathrm{h_f a_v}(\mathrm{T_s}-\mathrm{T})=\eta\rho_\mathrm{b}(-\Delta\mathrm{H})\mathrm{r_A}+k_{er}^{s}\left(\frac{\partial^2 T}{\partial r^2}+\frac{1}{r}\frac{\partial T}{\partial r}\right) \qquad \textbf{EQUATION 23}$$

where ε is the bed voidage, k_{er}^{f} and k_{er}^{s} are the effective thermal conductivities in the fluid and in the solid, and is the effectiveness factor (Froment & Bischoff, 1979). The effectiveness factor, defined in Equation 24, is a measure of the relative importance of diffusion and reaction limitations.

$$\eta=\frac{\text{Actual overall rate of reaction}}{\begin{array}{c}\text{Rate of reaction that would result if}\\ \text{entire interior surface were exposed}\\ \text{to external pellet surface conditions}\end{array}}=\frac{-\mathrm{r_A}}{-\mathrm{r_{As}}} \qquad \textbf{EQUATION 24}$$

All internal pellet gradients which were explicitly expressed in Equations 18 and 19 are lumped into the effectiveness factor.

Pedernera et. al (2003) employed a 2D heterogeneous model to analyze primary reformer performance in the steam reforming reaction. Using this model they were able to effectively compute radial temperature and reaction rate distributions throughout primary reformer tubes. The authors

concluded that the 2D heterogeneous model was a useful tool to identify problem zones within the catalyst bed and propose improvements to system design.

2.5. Computational Fluid Dynamics

Research into the mechanisms and behavior of physical phenomena such as fluid flow, heat and mass transfer, and chemical reaction have historically been divided into two distinct categories: pure theory and pure experiment. However the advent of powerful computing technology introduced a third and equally important category in fluid dynamics called computational fluid dynamics.

Computational fluid dynamics is a powerful tool which allows scientists to conduct numerical experiments in virtual laboratories. The use of CFD is widespread amongst many different industries, including the automobile, architectural, health, and chemical process industry. Despite its applicability to many different subject matters, one fact remains constant for all applications of CFD – it allows scientists to explore fluid flow phenomena without the great expense of creating costly experimental rigs. Furthermore, whereas a real-world experiment only allows one to observe parameters of interest at only a set number of points (limited by the location and capabilities of probes), CFD simulations provide continuous data with great resolution. Another great advantage of CFD is that the software can be run off of a thumb drive on any computer, or even on a terminal which can be accessed remotely by several users.

Despite the advantages of CFD there are inherent limitations to these simulations arising from potentially imprecise input data as well as deficiencies in the chosen mathematical model; therefore, CFD typically does not replace real-world experimentation entirely. Instead, because it provides a cheaper, faster, and more accessible alternative to experimentation, CFD simulations reduce the amount of experimentation which must be conducted and, therefore, the cost of projects.

2.5.1. CFD Problem Analysis

Figure 3 shows the sequential steps taken when using CFD to analyze a problem. The first four steps describe the preprocessing stage. First the problem must be clearly defined. This step calls for

information about the system such as the flow characteristics, composition of the fluid, and initial and boundary conditions. Next the user must choose a mathematical model to describe the system. Nearly all CFD applications make use of the Navier-Stokes equations, which are nonlinear partial differential equations (PDEs) that are difficult to solve analytically. The Navier-Stokes equations, when used together with other equations such as the conservation of mass, model fluid motion to an acceptable degree of accuracy and have been used for a range of flow conditions, including turbulent flow. The third step is for the user to construct the geometry of the system being analyzed. The user may use a number of different computer aided design programs such as AutoCAD, ProE, etc. After defining the geometric model, the user must then mesh it using a program such as GAMBIT. Meshing the geometric model creates small control volumes across which conservation of mass, momentum, and energy equations are solved. The final step in the preprocessing stage is to choose a CFD software package – Fluent was used in this study. The CFD software package interprets the meshed geometry and iteratively solves the mathematical models using the initial and boundary conditions specified.

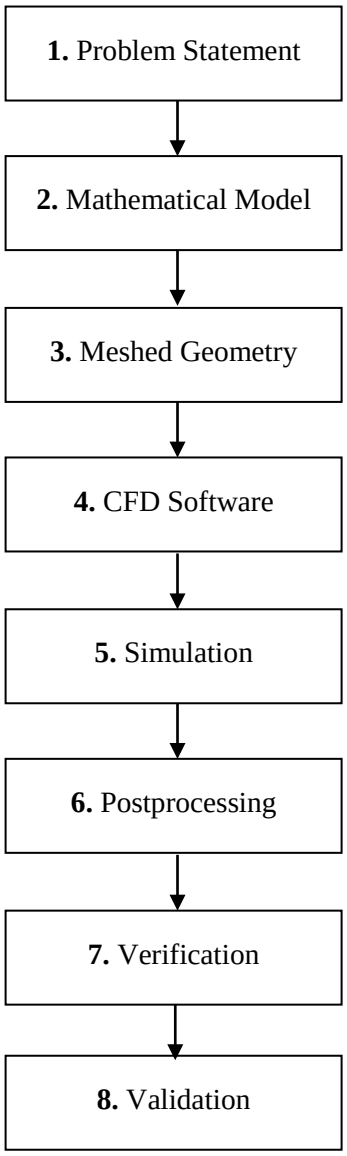

FIGURE 3: CFD ANALYSIS FLOWSHEET

The fifth step is the actual simulation of the system. The user must define several parameters within the CFD software such as the species present in the system, transport properties of said species, which equations the software must solve for, etc. The number of parameters which must be specified depends on the complexity of the system. After supplying all of the necessary information, the user initializes the simulation and sets how much iteration the software should complete. Furthermore the user specifies the convergence criteria for the simulation which, if met, will stop the simulation. After the simulation is complete, the user conducts post-processing where information about the system is available to the user for further analysis, often in graphical form.

The seventh step of the analysis process is to verify that the model was solved correctly. Verification of the model is accomplished by refining the mesh, running the simulation again, and comparing the results of the original mesh to the results of the refined mesh. The final step of CFD analysis is to validate the results of the simulation. This step is typically accomplished by comparing the results of the simulation to experimental data or to empirically-established correlations.

2.5.2. Theory of CFD

Three basic laws of conservation govern the fundamental equations which describe fluid dynamics: conservation of mass, conservation of momentum, and conservation of energy. The equation resulting from applying the conservation of mass to fluid flow is called the continuity equation (Tannehill, Anderson, & Pletcher, 1997). The conservation of momentum is simply Newton's Second Law, and when applied to fluid flow it results in a vector equation called the momentum equation. The conservation of energy equation is a restatement of the first law of thermodynamics, which states that the energy in the thermodynamic system of interest and its surroundings is conserved for any process.

According to Tannehill, Anderson, and Pletcher additional equations are necessary for the solution to a fluid dynamics simulation. One such equation is an equation of state which relates thermodynamic properties such as pressure (P), density (ρ), and temperature (T). Furthermore, when mass diffusion and chemical reaction occur within the system additional equations called the species continuity equations must also be included.

2.5.1.1. The Navier-Stokes Equations

When applied to an infinitesimal, fixed control volume, the continuity equation takes the following form:

$$\frac{d\rho}{dt} + \nabla \cdot (\rho \mathbf{V}) = S_m \qquad \textbf{EQUATION 25}$$

where **V** is the fluid velocity and S_m is a user-defined source term which accounts for any additions to the system via phase changes or other user-defined functions. In this study, as with most cases, the source term is taken to be zero. The first term in Equation 1.1 represents the rate of change in the density of the fluid, whereas the second term represents the rate of mass flux passing out of the control surface which bounds the control volume. In the Cartesian coordinate system Equation24 takes the following form:

$$\frac{d\rho}{dt} + \frac{\partial(\rho u)}{\partial x} + \frac{\partial(\rho v)}{\partial y} + \frac{\partial(\rho w)}{\partial z} = S_m \qquad \textbf{EQUATION 26}$$

where u, v, and w are the x, y, and z components of velocity, respectively. If the user-defined source term is taken to be zero and the flow is assumed to be incompressible (i.e. ρ is constant), Equation 24 can be further simplified:

$$\frac{\partial u}{\partial x} + \frac{\partial v}{\partial y} + \frac{\partial w}{\partial z} = 0 \qquad \textbf{EQUATION 27}$$

Thus for an incompressible fluid the continuity equation states that the sum of the fluid flow exiting the control volume must equal the sum of the fluid flow entering the control volume.

The conservation of momentum equation in the direction j takes the following form

$$\frac{\partial(\rho V_j)}{\partial t} + \nabla \cdot \left(\rho V_j \mathbf{V}\right) = -\frac{\partial p}{\partial x_j} + \frac{\partial \tau_{ij}}{\partial x_i} + \rho\, g_j + F_j \qquad \textbf{EQUATION 28}$$

where ρ is the density of the fluid, **V** and V_j are the velocity and j-component of the velocity, p is the static pressure, τ_{ij} is the surface stress acting on the fluid in direction j on a plane perpendicular to direction i, and ρg_j is the body gravitational force. The term F_i allows for the inclusion of additional body forces not already accounted for and is usually zero.

2.5.3. Spatial Discretization Methods

The partial differential equations which define the conservation of mass, momentum, energy, and species are solved in the integral form. These partial differential equations are continuous throughout the entire system domain (i.e. solutions exist at an infinite number of points), and simulation of even a simple

system would require a great amount of computational power. In order to reduce the required computational power all commercially available CFD codes utilize one of three spatial discretization methods: the finite difference (FD), finite element (FE), or finite volume (FV) method. All three of these methods employ equations which are analogous to the PDEs and whose domains are limited to a finite number of points.

The finite difference method is the oldest and most rigid of the three spatial discretization methods. This method requires the use of a structured grid, consisting of rectangular cells which can undergo only limited deformation, and is therefore difficult to apply to complex geometries. Figure 4 presents a sample grid which uses the FD method.

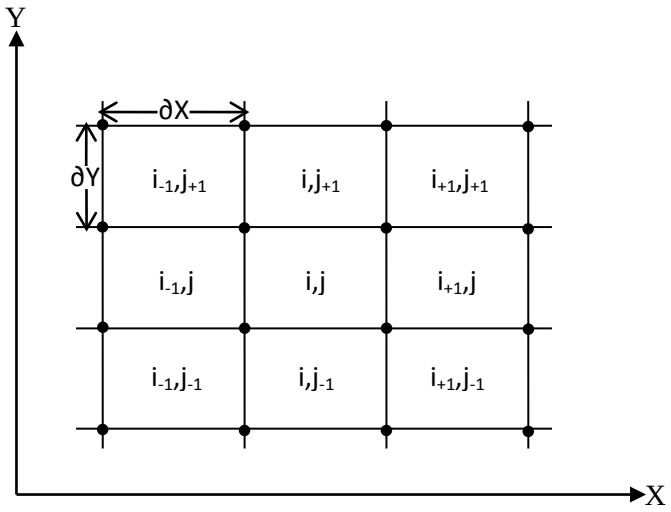

FIGURE 4: STRUCTURED, DISCRETE GRID RESULTING FROM APPLICATION OF THE FINITE DIFFERENCE METHOD

The FD method uses algebraic difference quotients (i.e. finite differences), typically determined by a Taylor series expansion, to provide a good approximation of the PDEs. Three common finite difference approximations are the first order forward, first order backward, and second order central differences. The first order forward and backward differences utilize information in one cell and the cell in front of it or the cell behind it, respectively, while the second order central difference uses both the cells in front of and behind of a known cell. These equations are given by:

First Order Forward Difference: $\left(\frac{\partial u}{\partial x}\right)_{i,j} = \frac{u_{i+1,j}-u_{i,j}}{\partial x} + O(\partial x)$ **EQUATION 29**

First Order Backward Difference: $\left(\frac{\partial u}{\partial x}\right)_{i,j} = \frac{u_{i,j}-u_{i-1,j}}{\partial x} + O(\partial x)$ **EQUATION 30**

Second Order Central Difference: $\left(\frac{\partial u}{\partial x}\right)_{i,j} = \frac{u_{i+1,j} - u_{i-1,j}}{2\,\partial x} + O(\partial x)^2$ **EQUATION 31**

Unlike the finite difference method, both the finite element and finite volume methods can be used to discretize unstructured grids. An unstructured grid consists of either two-dimensional triangular cell or three-dimensional tetrahedral cells distributed over the surface of a domain. Unlike the FD method, where the user strongly influences the grid structure, the FE and FV methods randomly generate cells throughout the domain. Although this randomness may seem less appealing than the exactness offered by a structured grid, it is the randomness of the discretization that allow the FE and FV methods to easily adapt to complex geometries. Both the FE and FV methods have their own strengths – the FE method is generally more accurate than the FV method, whereas the FV method solves a continuity balance for each control volume. Therefore the FV method is typically used in mass transport applications where maintaining the conservation of mass is highly important, whereas the FE method finds use in other applications such as the modeling of mechanical properties (e.g. stress) where maintaining the local continuity is less important.

2.5.4. Numerical Solutions

Solution to the conservation of momentum and other scalars such as mass and species are obtained in integral form in three steps. First the continuous domain is discretized into a finite number of control volumes defined by the system mesh. Then the system equations are integrated over the control volumes to generate algebraic equations for system variable such as velocity and species mass fraction. The final step is to solve the discretized equations.

Because the governing equations of the system are interdependent, the sequential iterative process outlined by Figure 5 is necessary to arrive at a converged solution (Nijemeisland & Dixon, 2001). First

the properties of the fluid are updated. For the case of the initial iteration the supplied initial conditions are used. The momentum equation is then solved using the current values for pressure and face mass flux. The velocities which result from solving the momentum equation may not satisfy the local continuity equation; therefore a 'Poisson-type' equation for pressure correction is derived using the continuity equation and a linearized continuity equation. Then the remaining equations, such as the conservation of energy and conservation of species, are solved and the fluid properties are updated. If the solution has not converged this process is repeated, otherwise the simulation stops.

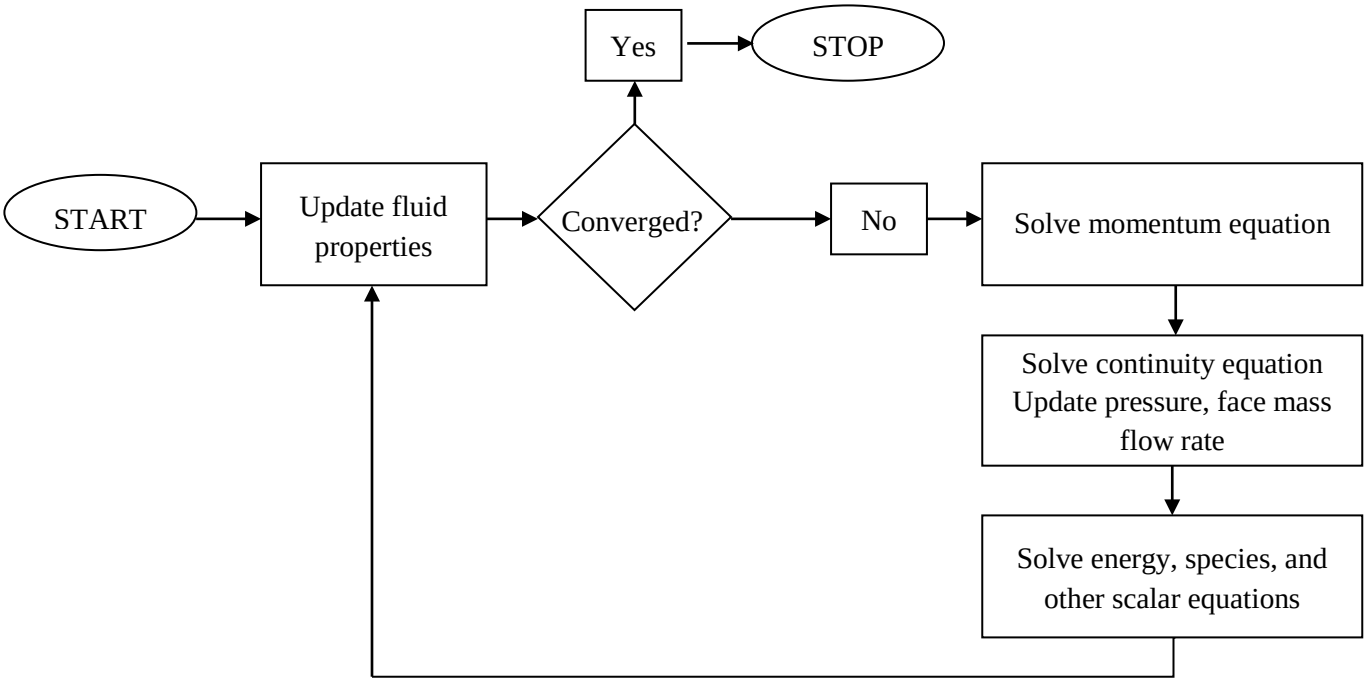

FIGURE 5: ITERATIVE SOLUTION PROCESS

2.5.5. Application of CFD to Chemical Reaction Engineering

One of the earliest applications of CFD to industrial problems used a two-dimensional model to study fixed-bed reactors (Dalman, Merkin, & McGreavy, 1986). Although the use of an axisymmetric radial plane severely limited the geometry of the system, this study provided realistic flow predictions thereby demonstrating that CFD is a useful tool to solve industrial problems.

As the computing power of commercially available hardware increased, simulations of increasingly complex systems became possible. Derkx and Dixon (1996) conducted one of the first 3D simulations of fixed-bed reactors using a model consisting of three spheres. This study showed how CFD could be used to obtain useful transport parameters such as the Nu_w numbers. Nijemeisland and Dixon (2001) built upon this research to develop a 44-sphere model to analyze heat transfer in a fixed bed. The authors demonstrated that, when designed properly, CFD simulations can provide results which both qualitatively and quantitatively fit experimental data. This study also demonstrated that when the limitations of the model are considered, a great deal of data can be obtained from CFD simulations.

Zieser et. al (2001) studied chemical reaction over a single particle in an inhomogeneous flow field. The results of the simulation showed that CFD can produce detailed pictures of concentration profiles around the particle in high resolution. The authors concluded that the inhomogeneity of the flow and concentration fields around the particle are significant and that more detailed models of external mass transfer may be necessary to accurately model diffusion and reaction in a catalyst pellet.

Significant research has been conducted on approximating diffusion and reaction parameters for 3D systems via simpler 1D and 2D models. Dixon and Cresswell (1987) showed that an infinitely long cylinder (1D) can be used to approximate effectiveness factors and pellet selectivities for a finite hollow cylinder (2D) model so long as an appropriate cylinder diameter is used for the 1D model. Burghardt and Kubaczka (1995) developed a model to approximate the effectiveness factor for any shape of a catalyst pellet by using a characteristic dimension of the catalyst pellet which describes the most probable pathway of diffusion of a reactant into the pellet. Additionally, Nagaraj and Mills (2008) simulated a wide variety of catalyst shapes in both 3D and 2D to demonstrate the many possibilities of current modeling software and techniques.

Recently CFD code has been applied to simple models which approximate transport in complex 3D geometries. Taskin et al. (2007) used a 120° wedge of a reactor tube to approximate reaction heat effects in a steam reformer tube. Mariani et al (2003) analyzed the effectiveness of the generalized cylinder (GC) model in approximating reaction in 3D pellet geometries at low reaction rates. The GC

model utilizes a shape parameter which can be determined by solving a Poisson equation. The study investigated several simple pellet geometries, including a one-hole, seven-hole, and multilobe pellet. The authors concluded the GC model accurately approximates overall reaction rates so long as the shape parameter is properly developed. The group built upon this research and also demonstrated the applicability of the GC model at high reaction rates (Mariani N. J., Keegan, Martinez, & Guillermo, 2008).

CHAPTER 3

Kinetic Experiments

In order to simulate the esterification reaction using Fluent and COMSOL, certain information regarding the kinetics of the reaction must be known. These parameters can be determined by observing how the concentration of reactants and products vary with time and then proposing a rate law to describe the mechanism of reaction.

3.1. Goals

The goals of the kinetic experiments described in this section are to propose a rate law for the esterification of methanol and acetic acid and to determine the activation energy and pre-exponential factor which describe this reaction.

3.2. Methodology

A dry mixture of 86 wt-% B-Zeolite powder, 10-wt% Cab-O-Sil and 4-wt% avecil was prepared. This mixture was placed into a plastic container with grinding media in it to ensure that it was thoroughly mixed. The mixture was then slurried to produce a wet, homogeneous solution. The slurried material was then dried in an oven for sixteen hours at a temperature of 100°C. The dried product was sieved to a size of less than 355 microns and then fired at 450°C for six hours (100°C/hr ramp) in order to maintain continuity with the method of producing a B-Zeolite catalyst pellet.

Figure 6 shows the experimental setup. Four grams of the fired product were added to a 250 ml round bottom flask with three necks (A). The central neck housed a reflux condenser (B) to trap any effluent gases and one side neck was fitted with a thermometer (C) to monitor the reaction temperature.

The third neck was fitted with a glass stopper (D) which could be removed to take samples from the reacting mixture.

The flask unit was suspended over a hot plate/stirrer (E) unit using clamps. The hot plate was set to a temperature of 20°C higher than the desired reaction temperature. The model used also had a temperature control unit (F) which maintained a steady heating media temperature (in this case silica oil). Experimentation showed that setting the temperature control unit to 5°C over the desired reaction temperature accounted for the heat losses within the system, allowing for the desired reaction temperature.

After the oil bath reached the appropriate temperature 180 ml of methanol and four grams of catalyst were added to the flask, which was then submerged in the heat bath. A small magnetic bar was added to the contents of the flask and the stirrer unit was set to spin at 850 rpm. When the liquid inside the flask reached the desired reaction temperature, 20 ml of acetic acid and 10 ml of 1,2,4-trichlorobenzene, which was used as an internal standard to conduct GLC analysis, were added. Samples were withdrawn every 30 minutes, filtered through a 0.2 micron syringe filter, and then diluted with acetone using a ratio of 9 parts acetone to 1 part filtered solution. This diluted solution was then sent for GLC analysis. Samples were withdrawn every 30 minutes for at least 180 minutes.

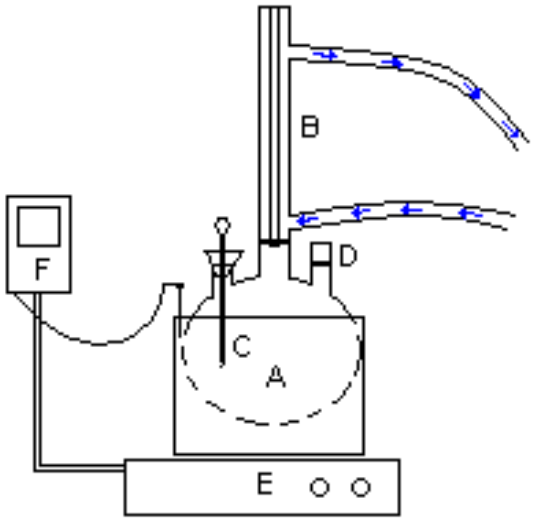

FIGURE 6: EXPERIMENTAL SETUP

3.3. Results

The results of gas-liquid chromatography analysis of the samples withdrawn from the reacting fluid are presented in Table 1.

TABLE 1: GAS-LIQUID CHROMATOGRAPHY ANALYSIS RESULTS

40°C 4g CATALYST			50°C 4g CATALYST			60°C 4g CATALYST			60°C 8g CATALYST		
Time (s)	$x_{Acetic\ Acid}$ (mol %)	$x_{Methyl\ Acetate}$ (%)	Time (s)	$x_{Acetic\ Acid}$ (mol %)	$x_{Methyl\ Acetate}$ (%)	Time (s)	$x_{Acetic\ Acid}$ (mol %)	$x_{Methyl\ Acetate}$ (%)	Time (s)	$x_{Acetic\ Acid}$ (mol %)	$x_{Methyl\ Acetate}$ (%)
0	9.09	0	0	9.5	0	0	9.5	0	0	9.5	0
1800	8.88	0.81	1800	10.55	0.87	1800	7.88	2.5	1800	7.9	4.58
3600	8.76	0.36	3600	9.81	1.8	3600	8.1	1.24	3600	6.52	6.91
5400	8.52	1.35	5400	9.18	2.27	5400	7.19	3.87	5400	5.24	9.01
7200	8.3	1.19	7200	8.85	2.57	7200	6.7	4.99	7200	4.21	9.95
9000	8.02	1.5	9000	8.54	3.37	9000	6.05	5.61	9000	3.41	10.57
10800	7.88	1.86	10800	8.71	2.72	10800	5.49	6.84	10800	2.92	12.4
12600	7.64	2.09	12600	7.74	4.15	12600	5.15	6.35			
14400	7.56	1.92	14400	7.4	4.69						

3.4. Discussion

Because methanol was present in excess the reaction can be approximated as a pseudo-first order reaction given by Equation 32.

$$r_{\text{acetic acid}} = -k' C_{\text{acetic acid}} \qquad \textbf{EQUATION 32}$$

where k' is a pseudo-first order rate constant defined as

$$k' = kC_{\text{methanol},0} \qquad \textbf{EQUATION 33}$$

By calculating the initial moles of each species present at $t = 0$, the total number of moles given by the GLC data at $t = 0$ can be verified.

$$N_{i,0} = x_{i,0} N_{tot} = \frac{\frac{V_{i,0}}{MW_i}}{\rho_i} \qquad \textbf{EQUATION 34}$$

Table 2 presents these calculations for each species present in the reaction vessel.

TABLE 2: KINETIC EXPERIMENT INITIAL CONDITIONS

Species	Density ($\frac{g}{cm^3}$)	Molecular Weight ($\frac{g}{mol}$)	Molar Volume ($\frac{cm^3}{mol}$)	Initial Volume (cm^3)	Initial Moles	Initial Mole Percent
Methanol	0.791	32.04	40.51	180	4.444	91.18
Acetic Acid	1.049	60.05	57.25	20	0.3494	7.169
Methyl Acetate	0.932	74.08	79.48	0	0	0.0000
Water	1	18.00	18.00	0	0	0.0000
1,2,4-trichlorobenzene	1.46	181.5	124.3	10	0.08046	1.651

dV ($\frac{cm^3}{mol}$)	Total Initial Volume (cm^3)	Total Initial Moles
-0.2716	210	4.874

As an example, consider the concentration of acetic acid at time $t = 0$ for the experiment at 40°C with four grams of catalyst. The total number of moles present in the system according to the experimental data is

$$N_{tot} = \frac{0.3494}{0.0909} = 3.843 \text{ moles}$$

However it is known that the total number of moles in the system at this time is 4.874 moles. Therefore the GLC data needed to be corrected by using Equation 35.

$$x_{i,corrected} = x_{i,experimental} \frac{x_{acetic\ acid,theoretical} + x_{methyl\ acetate,theoretical}}{x_{acetic\ acid,experimental} + x_{methyl\ acetate,experimental}} \quad \textbf{EQUATION 35}$$

This method scales the experimental results such that the initial theoretical concentration is never exceeded while maintaining the experimental trend. The next step in converting the experimental mole fraction data into concentration data is to calculate the volume of the species at every sampling time. Because the volume of the system decreases by 0.2716 cm^3 per mole of acetic acid which has reacted, it is necessary to know the overall conversion at each data point.

$$X = \left| \frac{x_i - x_{i,0}}{x_{i,0}} \right| \quad \textbf{EQUATION 36}$$

The volume of the system at each data point can then be calculated by

$$V = V_0 - X * N_0 * dV \quad \textbf{EQUATION 37}$$

As the total number of moles in the system remains constant, the concentration of species i can be calculated by Equation 38.

$$C_i = \frac{x_i N_0}{V} \quad \textbf{EQUATION 38}$$

The concentration data for each reactant and product are tabulated in Appendix A. The pseudo-first order rate constant can be obtained by plotting $\ln(C_i)$ against time for each run as done in Figure 7.

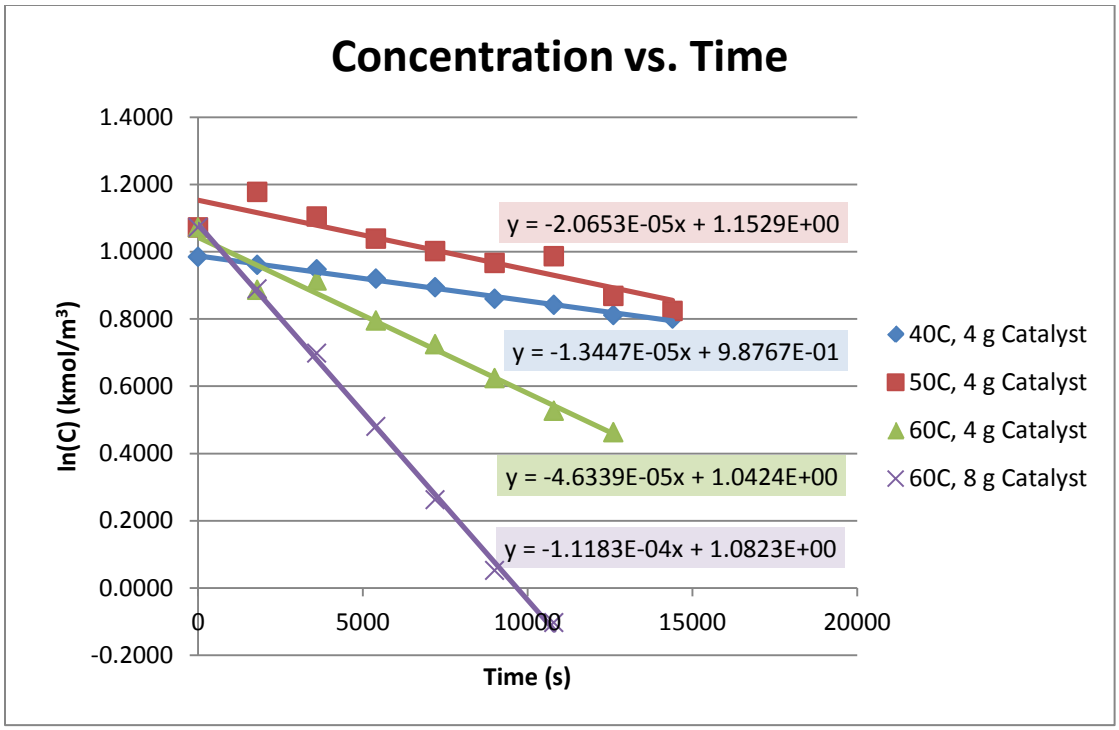

FIGURE 7: PSEUDO-FIRST ORDER RATE CONSTANT PLOT

The slopes of the linear trendlines in Figure 7 give the pseudo-first order rate constants, which have units of s^{-1}, for each experiment. However in both the failed MRI experiments and the computer simulations methanol was not present in excess. Therefore these pseudo-first order rate constants must be converted into second order rate constants by Equation 33. Table 3 presents he pseudo-first order rate constants and second order rate constants for each of the four experiments.

TABLE 3: PSEUDO-FIRST ORDER AND SECOND ORDER RATE CONSTANTS

Species	Pseudo-First Order Rate Constant $(\frac{1}{s})$	Second Order Rate Constant $(\frac{m^3}{kmol\ s})$
40°C, 4 g Catalyst	1.345 E-5	6.351 E-7
50°C, 4 g Catalyst	2.065 E-5	9.755 E-7
60°C, 4 g Catalyst	4.634 E-5	2.186 E-7
60°C, 8 g Catalyst	1.118 E-4	5.281 E-6

The temperature dependence of the second order rate constants is directly related to the activation energy, E_a, and pre-exponential factor, A of the reaction. Plotting the natural log of the rate constant against the inverse of temperature shows a linear relationship between these quantities. The second experiment at 60°C with a double charge of catalyst is not included in Figure 8 because it introduces reaction rate dependencies other than temperature.

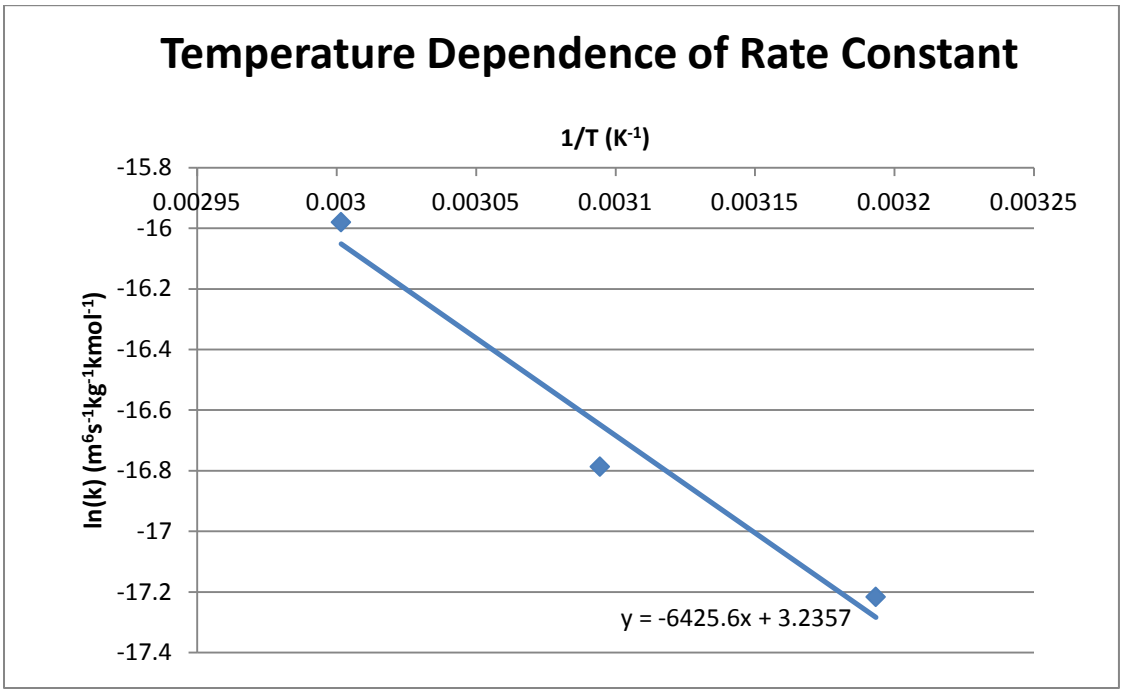

FIGURE 8: ARRHENIUS PLOT

The slope of the trendline in the Arrhenius plot is equal to $-\frac{E_a}{R}$ and the intercept is equal to ln(A), giving values of

$$E_a = 53.425\ \frac{kJ}{mol}$$

$$A = 25.424\ \frac{m^6}{kmol\ s\ kg_{catalyst}}$$

These two terms can be used to describe the rate constants for the given reaction at any temperature by means of the Arrhenius equation which is defined as

$$k(T) = A\exp\left(\frac{-E_a}{RT}\right) \qquad \textbf{EQUATION 39}$$

Table 4 compares the experimentally observed and theoretically predicted second order rate constants for the esterification reaction, both in terms of pellet volume and catalyst weight.

TABLE 4: EXPERIMENTAL AND PREDICTED SECOND ORDER RATE CONSTANTS FOR ESTERIFICATION OF ACETIC ACID AND METHANOL

Kinetic Parameter	Experimental Value	Predicted Value	Percent Difference	Experimental Value	Predicted Value	Percent Difference
	$\left(\frac{m^3}{kmol\ s}\right)$		(%)	$\left(\frac{m^6}{kmol\ s\ kg_{catalyst}}\right)$		(%)
k(40°C, 4 g catalyst)	$6.351*10^{-7}$	$5.938*10^{-7}$	6.50	$3.335*10^{-8}$	$3.118*10^{-8}$	6.51
k(50°C, 4 g catalyst)	$9.755*10^{-7}$	$1.120*10^{-6}$	14.81	$5.121*10^{-8}$	$5.883*10^{-8}$	14.88
k(60°C, 4 g catalyst)	$2.186*10^{-6}$	$2.035*10^{-6}$	6.91	$1.148*10^{-7}$	$1.069*10^{-7}$	6.88

Table 4 demonstrates that the values for the activation energy and pre-exponential factor used to calculate theoretical rate constants offer a good approximation of the experimental rate constants. The smallest error between experimental and theoretical values occurs at 40°C, therefore this is the temperature at which the simulations will be conducted.

CHAPTER 4

Methodology

The computer aided design software Gambit 2.4.6 was used to generate and mesh the reactor and pellet geometries. The computational fluid dynamics software package Fluent 6.3.26 was used to conduct three-dimensional modeling of diffusion and reaction in the catalyst system. The multiphysics software package COMSOL 3.5a was used to conduct one-dimensional modeling of diffusion and reaction in the catalyst system.

4.1 System Design

The system under investigation consists of a cylindrical reactor which contains one catalyst pellet. Reactants enter through the bottom of the reactor and flow over the catalyst pellet, where the reaction takes place, and the fluid exits through the top of the reactor.

4.1.1. Generating the System Geometry

The geometry of the pellet was chosen based on a commercially available catalyst pellet. The pellet, shown in Figure 9a, is cylindrical with four circular holes cut out of its interior and four semi-circular flutes cut out of its edges. Figure 9b shows the entire system, with the pellet inside of the cylindrical reactor.

The pellet has a diameter of 35 mm where no flutes exist and a diameter of 26.6 mm from flute to flute. The holes of the pellet are 8.5 mm in diameter and the pellet has a length of 10mm. The reactor is cylindrical with a diameter of 40 mm and a length of 270 mm. The catalyst pellet is positioned 70 mm above the reactor inlet.

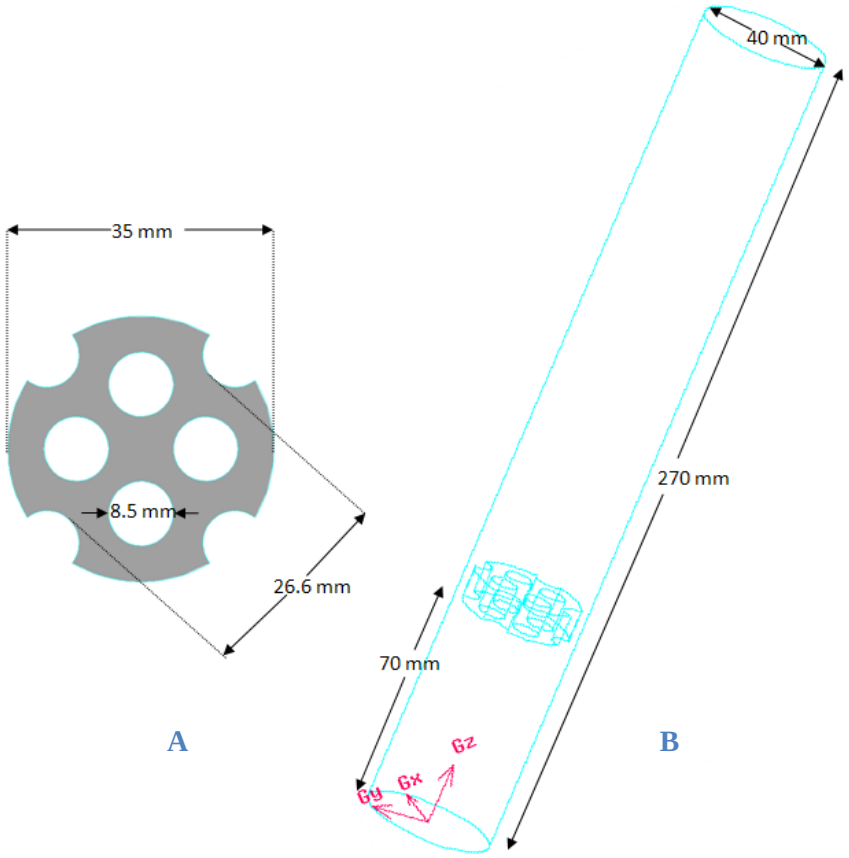

FIGURE 5: A. CATALYST PELLET B. SIMULATION SYSTEM

Because Gambit will not allow two volumes to occupy the same region, it was necessary to subtract the pellet volume from the reactor volume while retaining the pellet volume. This volume subtraction resulted in two faces, one belonging to the reactor (the fluid face) and one belonging to the pellet (the solid face). In order to properly mesh the geometry, these faces needed to be connected. After making all of the necessary connections, each face in the system was labeled.

4.1.2. Generating the System Mesh

The system mesh is shown in Figure 10. Because the faces of the pellet are regions of particular interest, they were meshed using a triangular scheme and an interval size of 0.0005 m, resulting in between 4500 and 12000 cells per face depending on the size of the face. The solid and fluid volumes were then meshed to include 254,266 and 171,209 cells, respectively. These meshing settings result in a much finer mesh on the catalyst pellet than in the other regions of the system. However, because all of the activity of interest occurs within the catalyst pellet, the less-refined mesh in the fluid region is acceptable.

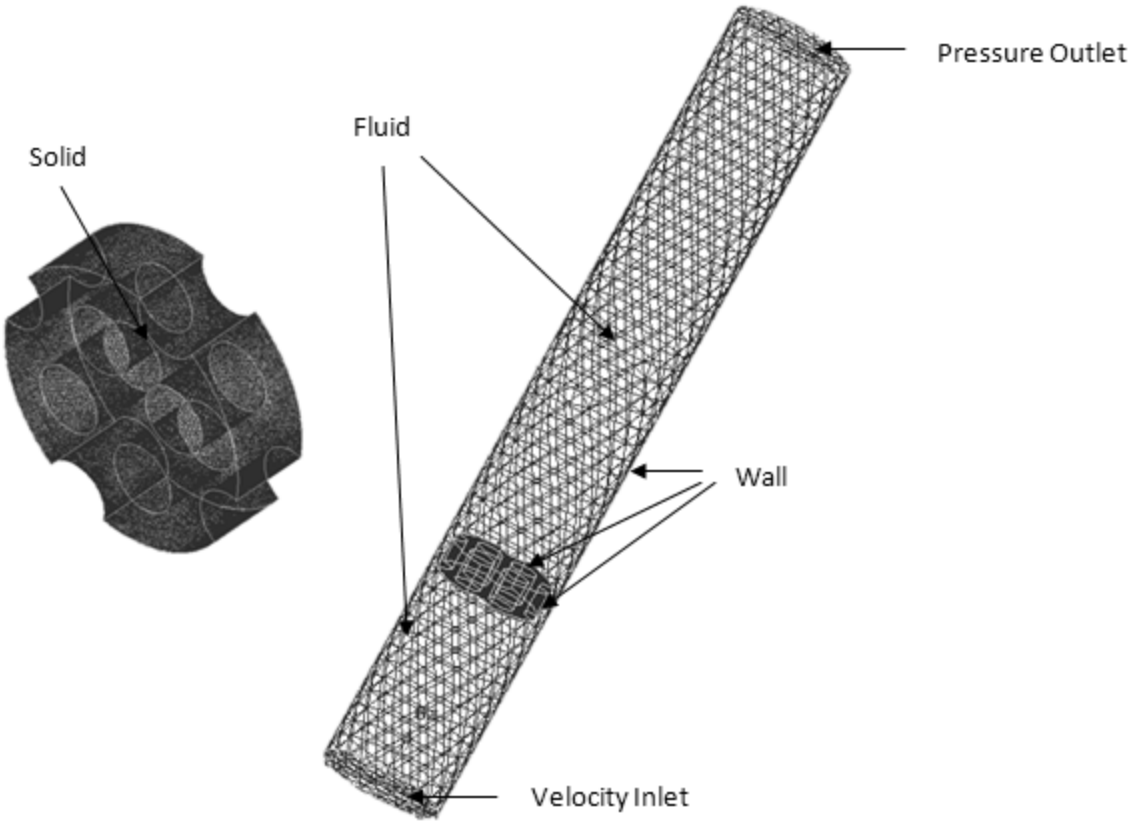

FIGURE 10: CATALYST SYSTEM MESH AND BOUNDARY CONDITIONS

4.1.3. Specifying the Geometry Boundary and Continuum Conditions

The final step in designing the system was to specify the boundary and continuum conditions for the different regions which exist within the system (these specifications are present in Figure 10).The bottom and top of the reactor were designated as the velocity inlet and pressure outlet, respectively, of the system. The reactor wall was specified as a wall, and the pellet faces were grouped together in a separate well designation. The reactor volume was specified as a fluid continuum, whereas the pellet volume was specified as a solid continuum.

4.2. Computational Fluid Dynamics Modeling

Fluent 6.3.26 was the computational fluid dynamics software used to simulate the catalyst-reactor system generated in Gambit. Several user-defined functions were used in order to accurately model the

reaction kinetics. Any specifications not discussed below can be assumed to have a default value in Fluent.

4.2.1. Use of User Defined Scalars

In Fluent, one can model a region as solid or porous (a porous region is treated as a fluid region). Because this system contains a catalyst pellet into which reacting species diffuse, the logical choice would be to model the pellet as porous. However, such a definition causes the undesirable error of non-zero velocity at the surface of the pellet (Dixon, Taskin, Nijemeisland, & Stitt, 2010). To avoid this error, the pellet can be modeled as a solid region in order to ensure that the no-slip boundary condition is met.

Choosing to model the pellet as solid rather than porous introduces additional complexities to the simulation. These complexities arise from the fact that Fluent does not allow for species to exist within a solid material. Therefore user defined scalars (UDS) must be implemented to calculate the appropriate mass fraction of species entering the material using information available from the adjacent fluid regions. Furthermore, UDS must be implemented to simulate reaction within the pellet, calculate the flux of species out of the pellet, and then couple that information to the adjacent fluid regions so that the mass fraction of species in the fluid surrounding the pellet is correct.

4.2.2. System Definitions

Fluent's pressure based solver was used in three-dimensional mode under steady-state conditions. The velocity formulation was taken to be absolute, the solution was set to be implicit, and the porous formulation was set to superficial velocity. The default choice of Green-Gauss cell based gradient option was used. Only the flow, which was laminar, and UDS equations were solved for.

The fluid region of the system contains four liquid species which were defined under the materials tab as a mixture. Ideal behavior of this liquid mixture was assumed, and the heat capacity, thermal conductivity, energy, and viscosity of the mixture were taken to be constant as very low conversions of species were expected. Similarly, the heat capacity, thermal conductivity, and density of the solid were also taken to be constant. Table 5 presents the physical property data of the fluid and solid,

as well as the reactor conditions. The solid properties were taken to be those of porous alumina due its similarity to silica structures and the absence of experimental data for the β-zeolite.

TABLE 5: MATERIAL AND REACTOR DEFINITIONS (FLUENT)

FLUID PROPERTIES

Thermal Conductivity, k $(\frac{W}{m\ K})$	Heat Capacity, C_P $(\frac{J}{kg\ K})$	Viscosity, μ $(\frac{kg}{m\ s})$
0.198	2292	8 E-4

SOLID PROPERTIES

Thermal Conductivity, k $(\frac{W}{m\ K})$	Heat Capacity, C_P $(\frac{J}{kg\ K})$	Density, ρ $(\frac{kg}{m^3})$
1	1000	1947

REACTOR CONDITIONS

Inlet Temperature (K)	Inlet Velocity $(\frac{m}{s})$	Operating Pressure (atm)
313.15	2.056 E-2	1

The fluid mixture consisted of four species: methanol, acetic acid, methyl acetate, and water. The mass diffusivities of these species were specified as dilute-approx and the UDS diffusivities of these species were given by user defined functions. In a system of n species, only n-1 species must be completely specified in Fluent in order to reach a solution – the final species is calculated by closing mass balances. Table 6 presents the three specified species in the system and their corresponding user defined scalar number, mass diffusivities, mass fraction, and UDS value at the inlet.

TABLE 6: SPECIES MASS DIFFUSIVITIES AND INLET BOUNDARY CONDITIONS

Species	User Defined Scalar Number	Mass Diffusivity ($\frac{m^2}{s}$)	Inlet Mass Fraction	Inlet UDS
Methanol	0	3.5531 E-9	0.347827	0.347827
Methyl Acetate	1	7.1960 E-9	0	0
Water	2	1.9745 E-9	0	0
Acetic Acid	N/A	1.5886 E-9	N/A	N/A

Because of the use of UDS which describe the mass fraction of methanol, methyl acetate, and water, UDS 0 through 2 must be defined to have a specified value at the velocity inlet equal to the desired inlet mass fraction. Any discrepancy between the mass fraction and UDS within the system can cause errors in the simulation. The UDS code was interpreted with a stack size of 10000 and the user defined function hook labeled adjust was set to Yi_adjust (the section of the C code which couples the species mass fractions within the pellet to the species mass fractions in the bulk fluid).

The reactor walls were specified as stationary walls which satisfy the no-slip shear condition. The system is treated as adiabatic, so the heat flux across the walls was specified to be constant with a value of zero. Furthermore, because no species diffuse through the walls, the species were defined to have zero diffusive flux across the walls. Furthermore, as with the case for defining the inlet mass fractions, the UDS boundary conditions at the walls was defined to have a constant specified flux of zero.

The pellet wall and was specified as a stationary wall which satisfies the no-slip shear condition. The heat flux across the pellet wall and its shadow was specified as a coupled flux, and the heat generation was set to a constant value of zero. Because Fluent does not allow species to exist within solid regions, the species were defined to have zero diffusive flux across the wall of the pellet. Each UDS was defined to have a specified value given by the user-defined function uds_coupled_i (where i corresponds to the appropriate UDS number).

4.2.3 Simulation Solving

The system was initialized to the settings shown in Table 7.

TABLE 7: INITIALIZATION CONDITIONS (FLUENT)

SPECIES			VELOCITY			REACTOR CONDITIONS	
Species	Mass Fraction	UDS Value	V_X $(\frac{m}{s})$	V_Y $(\frac{m}{s})$	V_Z $(\frac{m}{s})$	Gauge Pressure (Pa)	Temperature (K)
Methanol	0.347827	0.347827	0	0	0.02	0	313.15
Acetic Acid	0	0					
Water	0	0					

4.3. Multiphysics Modeling

The chemical engineering/mass transfer/diffusion/steady state package in one dimension was the package loaded into COMSOL 3.5a to simulate the catalyst pellet in one-dimension.

4.3.1. System Geometry and Mesh

Modeling the catalyst pellet as a sphere in one dimension requires only a line whose length is equal to the equivalent radius of the three-dimensional pellet. In this study three different equivalent radii were investigated – one which gave the same spherical ratio of volume to surface are as that of the pellet (r = 0.00525 m), one which gave the same volume as the pellet (r = 0.011406 m), and one which gave the same surface area of the pellet (r = 0.016796 m). The geometry of the one-dimensional model is significantly simpler than the geometry of the three-dimensional model as it consists only of a line, representing the radius of the sphere, discretized into 480 finite elements. A section of the mesh is shown in Figure 11 so that individual elements are apparent.

FIGURE 11: COMSOL SYSTEM GEOMETRY AND MESH

4.3.2. System Definitions

Under the subdomain settings tab, COMSOL informs the user that the equation which it will be solving to simulate reaction and diffusion is given by

$$\nabla \cdot (-D_e \nabla C) = R \qquad \textbf{EQUATION 40}$$

In one dimension this equation reduces to

$$-\frac{d}{dx}\left(D\frac{dC}{dx}\right) = R \qquad \textbf{EQUATION 41}$$

Because only the forward reaction is considered in this study, the reaction rate was a nonlinear function of the concentration of reactants. Because the concentration of methanol and acetic acid are equal in the bulk fluid, the relationship between diffusion and reaction can be written as

$$\frac{1}{r^2}\left(D_e r^2 \frac{dC}{dr}\right) = kC_{methanol}^2 \qquad \textbf{EQUATION 42}$$

where r is radial position, c is concentration, k is the rate constant, and D_e is the effective diffusivity. Equation 42 can be expanded to yield

$$D_e\left(\frac{2}{r}\frac{dC}{dr} + \frac{d^2C}{dr^2}\right) = kC_{methanol}^2 \qquad \textbf{EQUATION 43}$$

Next the boundary conditions were specified. In order to properly define the boundary condition at the surface of the pellet, as mass transfer coefficient was used to account for diffusion from the bulk fluid into the pellet. Two mass transfer coefficients were evaluated for each model, the first obtained from the three-dimensional simulations and the second calculated using a theoretical correlation. The theoretical correlation for the mass transfer coefficient for flow around a single sphere makes use of the Sherwood number, which can be calculated using Equation 2.

$$Sh = 2 + 0.6Re^{1/2}Sc^{1/3} = 2 + 0.6\left(\frac{\rho D v}{\mu}\right)^{1/2}\left(\frac{\mu}{\rho M}\right)^{1/3}$$

$$= 2 + 0.6\left(\frac{923 * 0.04 * 0.02056}{0.0008}\right)^{1/2}\left(\frac{0.0008}{939.6 * 2.6369 * 10^{-9}}\right)^{1/3} = 129.5$$

where ρ is the density in $\frac{kg}{m^3}$, D is the diameter of the reactor in m, μ is the viscosity of the fluid in $\frac{kg}{m\,s}$, and M is the mass diffusivity of the fluid in $\frac{m^2}{s}$. Knowing the Sherwood number and defining the characteristic length of the spherical pellet to be the ratio of the volume to surface area of the actual pellet allows the calculation of the mass transfer coefficient.

$$k_c = \frac{Sh\ M}{L} = \frac{127.1 * 2.6369 * 10^{-9}}{0.00175} = 1.953 * 10^{-4}\ \frac{m}{s}$$

The boundary condition on one side of the pellet was defined in terms of flux, utilizing the mass transfer coefficient and bulk concentration, in order to determine if external diffusion could be neglected. The boundary condition at the other side of the pellet was defined such that there was no flux through the center of the pellet.

CHAPTER 5

Results

5.1. 3D CFD Model

This section describes the results of the computational fluid dynamics modeling of diffusion and reaction within the three-dimensional catalyst model described in Chapter 4.

5.1.1. CFD Model Verification

The system mesh was refined to determine whether or not the original mesh density provided accurate results. The numbers of mesh elements for the original and refined meshes, as well as the corresponding overall reaction rates and molar flow rates of methanol, are presented in Table 8. Each system was simulated for 250 iterations, after which no improvement in convergence or change in results occurred.

TABLE 8: COMPARISON OF ORIGINAL AND REFINED MESH SIMULATION RESULTS

System	Number of Solid Mesh Elements	Number of Fluid Mesh Elements	Overall Reaction Rate ($\frac{kmol}{s}$)	Methanol Molar Flow Rate ($\frac{kmol}{s}$)
Original	254,266	171,209	1.66828E-8	-1.47504E-8
Refined	486,139	327,170	1.67782E-8	-1.48472E-8

Despite nearly doubling the number of elements in both the solid and fluid regions, the overall reaction rate and molar flow rate of methanol predicted by the original and refined system are very similar – the difference in overall reaction rate and molar flow rate of methanol predicted by both systems amounts to only 0.572% and 0.656% of the results given by the original system, respectively. The results presented in the rest of this chapter utilize the original system mesh because it is less computationally

taxing than the refined system and provides similar results. Plots showing residual values for both the original and refined meshes are provided in Appendix C.

5.1.2. Overall Reaction and Molar Flow Rates

At equilibrium the rate of reaction inside the pellet should equal the molar flow rate of species out of the pellet. Both of these rates were calculated using define on demand functions and are shown in Table 9.

TABLE 9: OVERALL RATE OF REACTION AND MOLAR FLOW RATE FOR 3D MODEL

Species	Rate of Reaction $(\frac{kmol}{s})$	Molar Flow Rate $(\frac{kmol}{s})$
Methanol	-1.66828 E-8	-1.47504 E-8
Methyl Acetate	1.66828 E-8	1.47504 E-8
Water	1.66828 E-8	1.47503 E-8

The conservation of mass is satisfied if the molar flow rate of reactants into the pellet equals the molar flow rate of products out of the pellet, as is the case for this system. Furthermore, the rate of consumption of reactants equals the rate of generation of products, as would be expected. However, under equilibrium conditions the rate of reaction should equal the molar flow rate out of the pellet for each species. For this simulation, the molar flow rate out of the pellet for any given species equals 88.5% of the rate of reaction within the pellet. This difference between the molar flow rate and rate of reaction indicates that the results of this simulation are relatively accurate, yet the possible 11.5% error in results demonstrates room for improvement in the model.

Both diffusion and reaction limitations affect the overall rate of reaction. The internal effectiveness factor for this system is equal to 0.4271, indicating that the system limitations are neither overwhelmingly due to diffusion nor reaction. Instead, the limitations of diffusion and reaction both play important roles in controlling the overall rate of reaction in the system.

5.1.3. Characterization of Pellet Surface

The surface mass fractions of methanol and methyl acetate are shown in Figure 12. Calculating the average mass fraction of methanol on the surface by integrating over the pellet surface resulted in a concentration of methanol on the pellet surface equal to 10.09 $\frac{\text{kmol}}{\text{m}^3}$. When compared to the concentration of methanol in the bulk fluid, which equaled 10.21 $\frac{\text{kmol}}{\text{m}^3}$, it is clear to see that there is no sharp concentration gradient at the pellet surface, and therefore the rate of reaction at the pellet surface is relatively slow. The flux of methanol into the pellet, calculated by a define on demand function, equaled 4.12577- 6 $\frac{\text{kmol}}{\text{m}^2\text{s}}$. The low molar flux of methanol into the pellet and the small difference in methanol surface and bulk fluid concentrations indicate a resistance to external mass transfer, represented by the mass transfer coefficient which was calculated as

$$k_c = \frac{W_{methanol}}{(C_{methanol,bulk} - C_{methanol,surface})} = 3.438\text{E-}5\ \frac{\text{m}}{\text{s}}$$

Furthermore, the catalyst edges appear to be poor regions for the reactants to diffuse into the pellet. The user-defined source code which governs the diffusion and reaction of species into the pellet utilizes

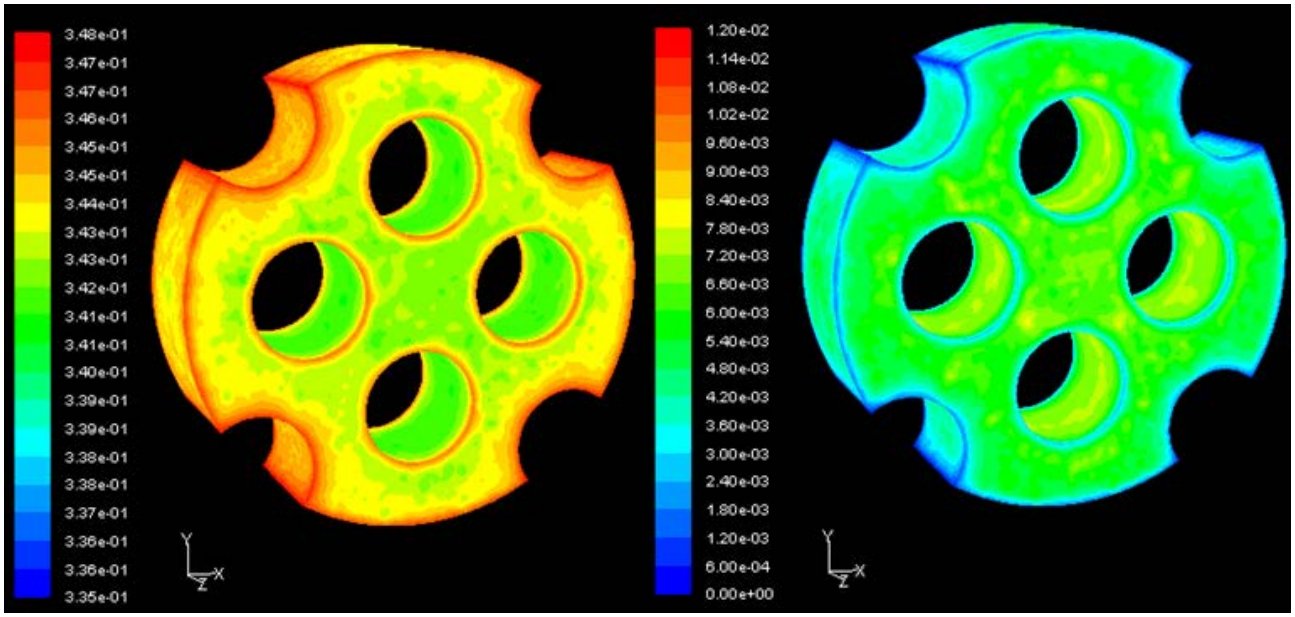

FIGURE 12: METHANOL (LEFT) AND METHYL ACETATE (RIGHT) SURFACE MASS FRACTION CONTOUR PLOTS

vectors normal to the faces of the pellet. Because the edges of the pellet are not faces themselves, but rather join two faces, it is likely that no species diffuse through them. Any products which result from reaction along the edges join the bulk fluid and are quickly replaced by reactants.

5.1.4. Characterization of Pellet Internals

The variation of methanol and methyl acetate mass fraction throughout two planes which intersect the catalyst pellet is shown in Figure 13. Regions of high methanol mass fraction correspond to regions of low methyl acetate mass fraction, as expected. At the surface of the pellet the concentration of reactants, and therefore the reaction rate, is the highest, resulting in the sharp change in both reactant and product species mass fractions from their respective bulk fluid values seen in Plane 1. The highest mass fraction of product species occurs in the center of the pellet. This concentration of product species at the center of the pellet is likely the result of internal diffusion limitations – reactants are unable to diffuse deep into the center of the pellet to replace the methanol and acetic acid which have been consumed.

The results shown in Plane 2 support this theory by showing that regions which have a high surface area to volume ratio show higher reactant mass fractions than regions with low surface area to volume ratios. For example, compare the region enclosed in dotted white rectangle to that enclosed in a solid white rectangle. The latter has more surface area for reactants to diffuse through due to the two holes which exist on either side of it, and correspondingly shows a higher amount of reactants than the former.

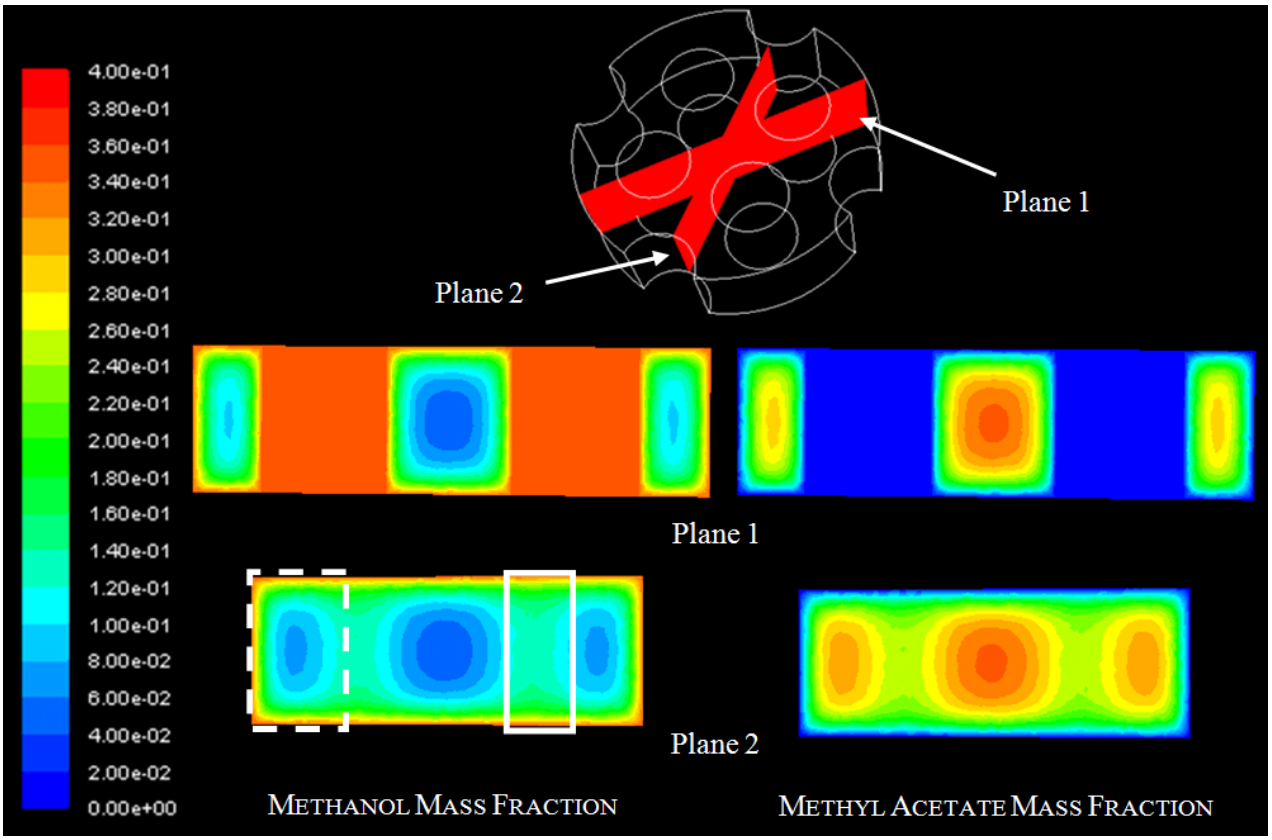

FIGURE 13: METHANOL MASS FRACTION CONTOUR PLOTS THROUGH PELLET

The dependence of product mass fraction on the axial position within the catalyst pellet is shown in Figure 14. Contour plots of methyl acetate mass fraction were produced for cross-sections of the pellet from just inside of the pellet (z = 0.0701 m) to halfway through the pellet (z = 0.075 m). In a system where there are no internal diffusion limitations the concentration of species within the pellet is uniform as reaction takes place at an equal rate throughout the pellet. Thus the presence of an internal concentration gradient, such as that seen in Figure 13, indicates the existence of internal diffusion limitations.

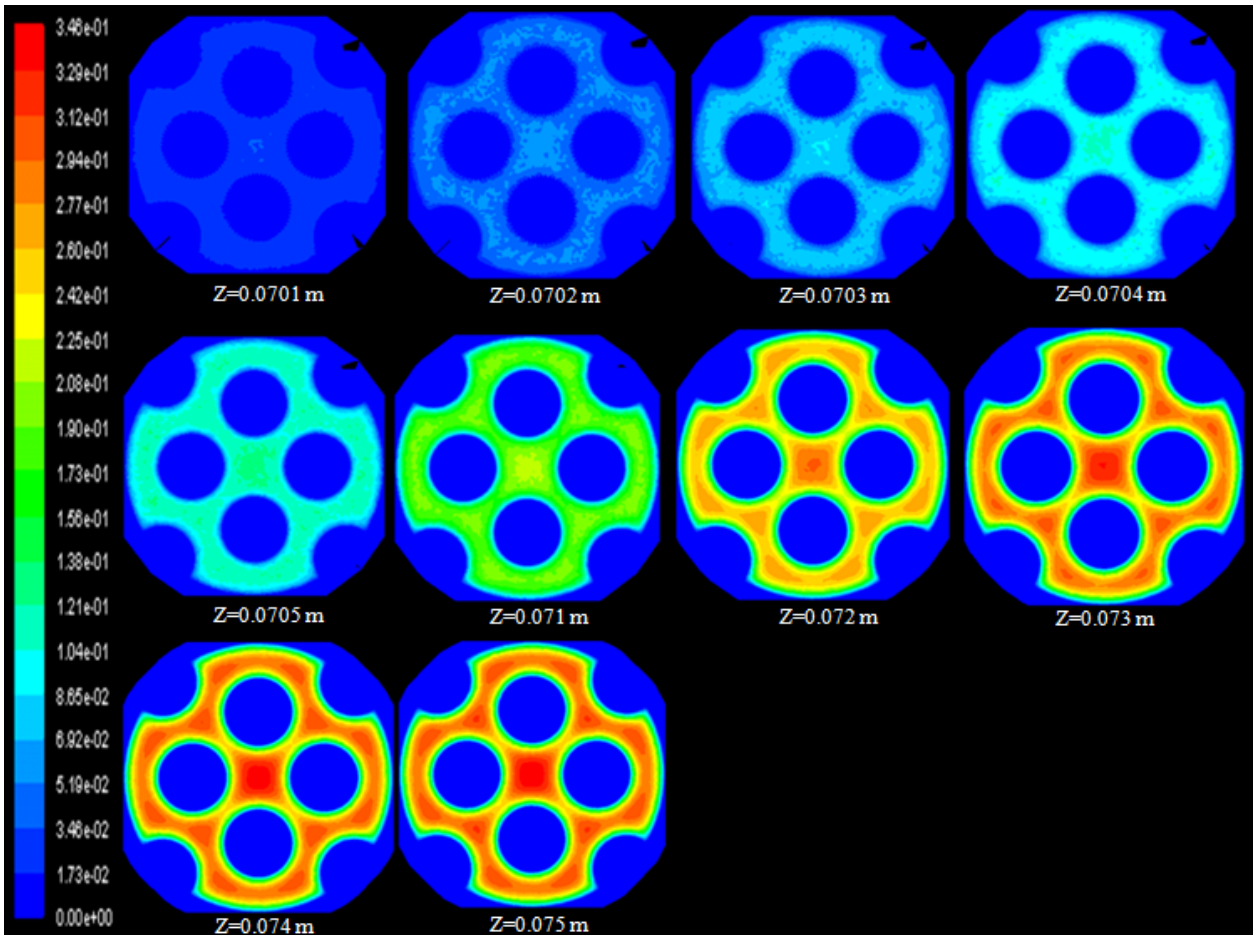

FIGURE 146: EFFECT OF INTERNAL DIFFUSION LIMITATIONS IN CATALYST PELLET

The internal limitations of the system were also tested by increasing the operating temperature (and therefore the reaction rate) while maintaining the original species diffusivities. Figure 15 shows the mass fraction of methanol through Plane 1 (see Figure 13) for two different operating temperatures.

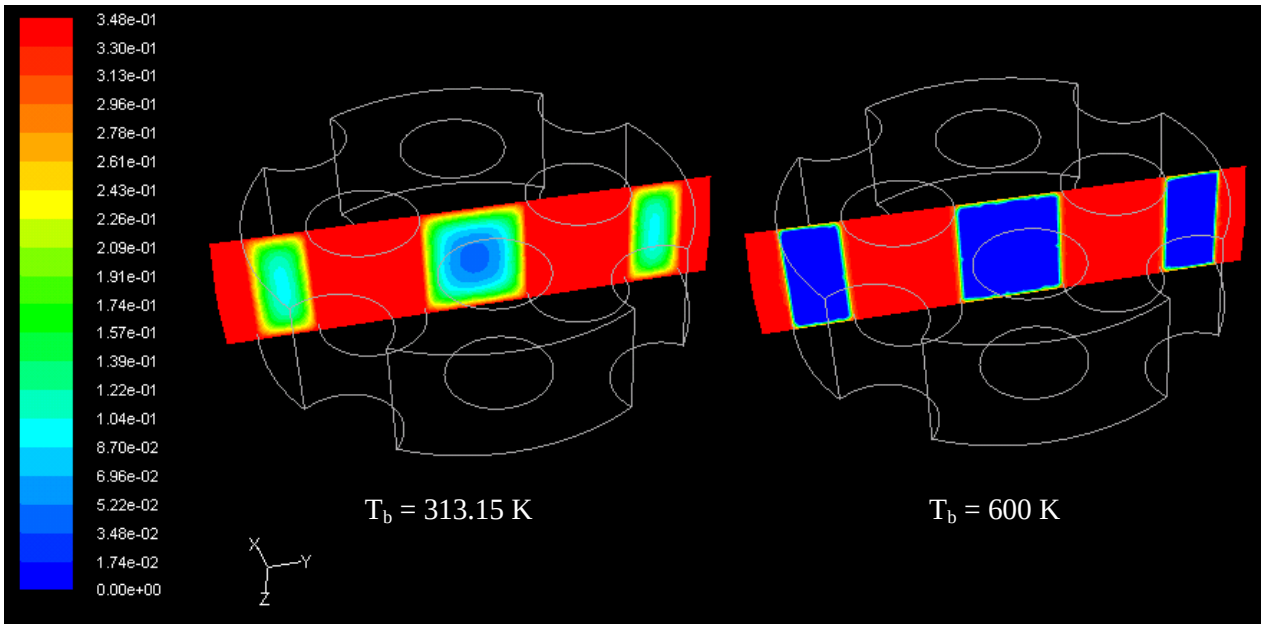

FIGURE 75: OPERATING TEMPERATURE DEPENDENCE OF METHANOL MASS FRACTION INSIDE PELLET

Figure 15 shows that when the bulk fluid temperature is increased from 313.15 K to 600 K all of the reaction occurs within the outermost layers of the catalyst pellet and no concentration gradient exists inside the pellet apart from surface regions. This comparison clearly shows that the system is limited by internal diffusion of reacting species.

5.1.5. Qualitative Validation of CFD Model

Although there is a lack of quantitative experimental data to compare the results of the simulation against, there is a modicum of qualitative data which was obtained from H-NMR analysis. Figure 16 compares the simulated mass fraction of methanol to the volume fraction of methanol obtained from H-NMR analysis of a catalyst pellet over which the esterification reaction was carried out. Although the similarity in qualitative results does not validate the results of the CFD simulation, it does lend some credibility to the CFD model.

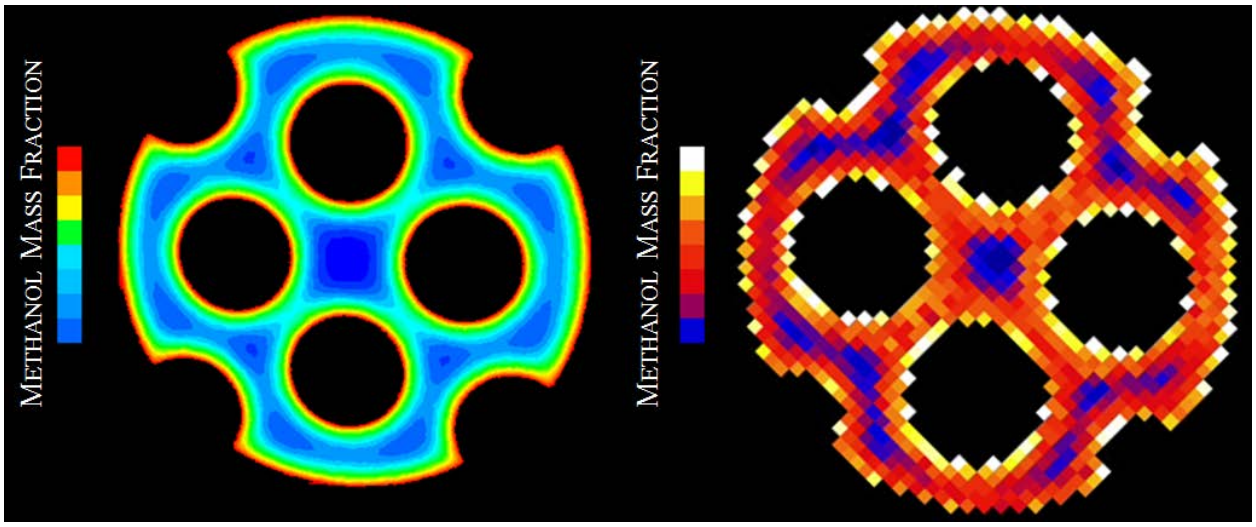

FIGURE 86: QUALITATIVE COMPARISON OF METHANOL MASS FRACTION BETWEEN 3D CFD RESULTS AND H-NMR ANALYSIS

5.2. 1D Multiphysics Model

Three different 1D models, each using a different equivalent spherical radius to approximate the 3D pellet geometry, were analyzed. The radii of the three models corresponded to a sphere with the same ratio of surface area to volume as the actual pellet (r = 0.00525 m), the same volume as the pellet (r = 0.011406 m), and the same surface area as the pellet (r = 0.016796 m).

5.2.1. 1D Model Verification

The mesh of each 1D model was refined to verify that an increase in mesh density did not affect the simulation results. Table 10 shows how increasing the number of mesh elements from 480 to 960 affected the molar flux of methanol at the pellet surface for each model.

TABLE 10: 1D MODEL VERIFICATION

	METHANOL MOLAR FLUX ($\frac{mol}{m^2 s}$)		
Number of Mesh Elements	**$V_s/S_s = V_p/S_p$ (R = 0.00525 m)**	**$V_s = V_p$ (R = 0.011406 m)**	**$S_s = S_p$ (R = 0.016796)**
480	0.003404	0.003674	0.003726
960	0.003404	0.003674	0.003727

The models which used radii of 0.00525 m and 0.011406 m showed no improvement with an increased mesh density. Increasing the number of mesh elements from 480 to 960 resulted in a slight change for the third model; however as this difference only amounts to 2.684E-4 of the result generated using 480 mesh elements, the original mesh was deemed suitable for simulation.

5.2.2. Overall Reaction Rates

It was suspected that external diffusion was negligible in the 1D simulations. In order to verify this assumption, the overall reaction rate for each of the three 1D models were evaluated under three different surface boundary conditions: setting the pellet surface concentration to the bulk fluid concentration with no mass transfer coefficient, using the mass transfer coefficient predicted by the Frössling correlation, and using the mass transfer coefficient calculated from the 3D simulation. Table 11 presents these results.

TABLE 11: 1D MODEL OVERALL REACTION RATES

	OVERALL REACTION RATE ($\frac{kmol}{s}$)		
k_c Used	**1D-1 (R = 0.00525 m)**	**1D-2 (R = 0.011406 m)**	**1D-3 (R = 0.016796)**
None	1.1492E-9	5.4735E-9	1.1231E-8
k_c from Sherwood	1.1461E-9	5.4588E-9	1.1202E-8
k_c from 3D Simulation	1.1340E-9	5.3983E-9	1.1082E-8

The greatest difference in results occurs between simulations which set the pellet surface concentration equal to the bulk fluid (i.e. no mass transfer coefficient) and those which use the mass transfer coefficient calculated from the 3D simulation. This difference amounts to less than 1.38% disagreement between overall reaction rates. Thus the assumption that external diffusion was negligible

was deemed appropriate and all 1D simulations were conducted without the use of a mass transfer coefficient.

5.2.3. Comparison to 3D Simulation

Table 12 compares the overall reaction rates predicted by the 3D model and 1D models.

TABLE 12: COMPARISON OF OVERALL REACTION RATES GIVEN BY 3D AND 1D SIMULATIONS

Simulation	Overall Reaction Rate ($\frac{kmol}{s}$)	% Difference from Overall Reaction Rate of 3D Simulation
3D	1.66828 E-8	0
1D-1 (R = 0.00525 m)	1.1492E-9	93.11%
1D-2 (R = 0.011406 m)	5.4735E-9	67.19%
1D-3 (R = 0.016796)	1.1231E-8	32.68%

All three 1D models yielded overall reaction rates lower than those given by the 3D simulation. The worst agreement was observed in the 1D model whose ratio of volume to surface area equaled that of the pellet, while the best agreement was observed in the 1D model whose surface area equaled that of the pellet. This result highlights the importance of surface area in catalyst design. Simulation 1D-3 had the highest surface area of any of the 1D simulations, thereby maximizing the area through which species could diffuse into the pellet and therefore react. Although one may expect simulation 1D-1 to show the best agreement with the 3D simulation, the small surface area of the sphere limits the overall reaction rate. Additionally, the fact that the only region through which species can react exists along the surface of the sphere (in contrast to the many possible regions in the 3D model introduced by the presence of holes and flutes) contributes to the lower observed overall reaction rates.

The variation of methanol with respect to relative radius for the 1D models is shown in Figure 17. The variation of methanol as a function of relative axial position, where z is axial position and L/2 is half

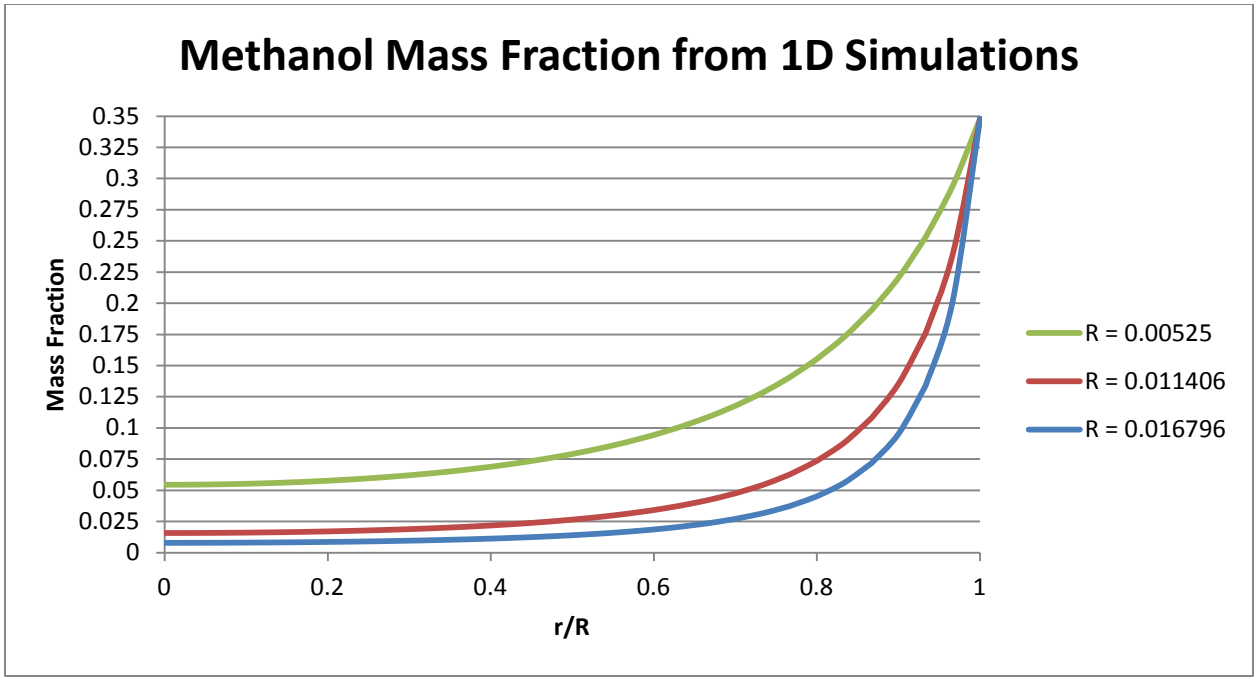

FIGURE 97: RADIAL PROFILE OF METHANOL MASS FRACTION FOR 1D SIMULATIONS

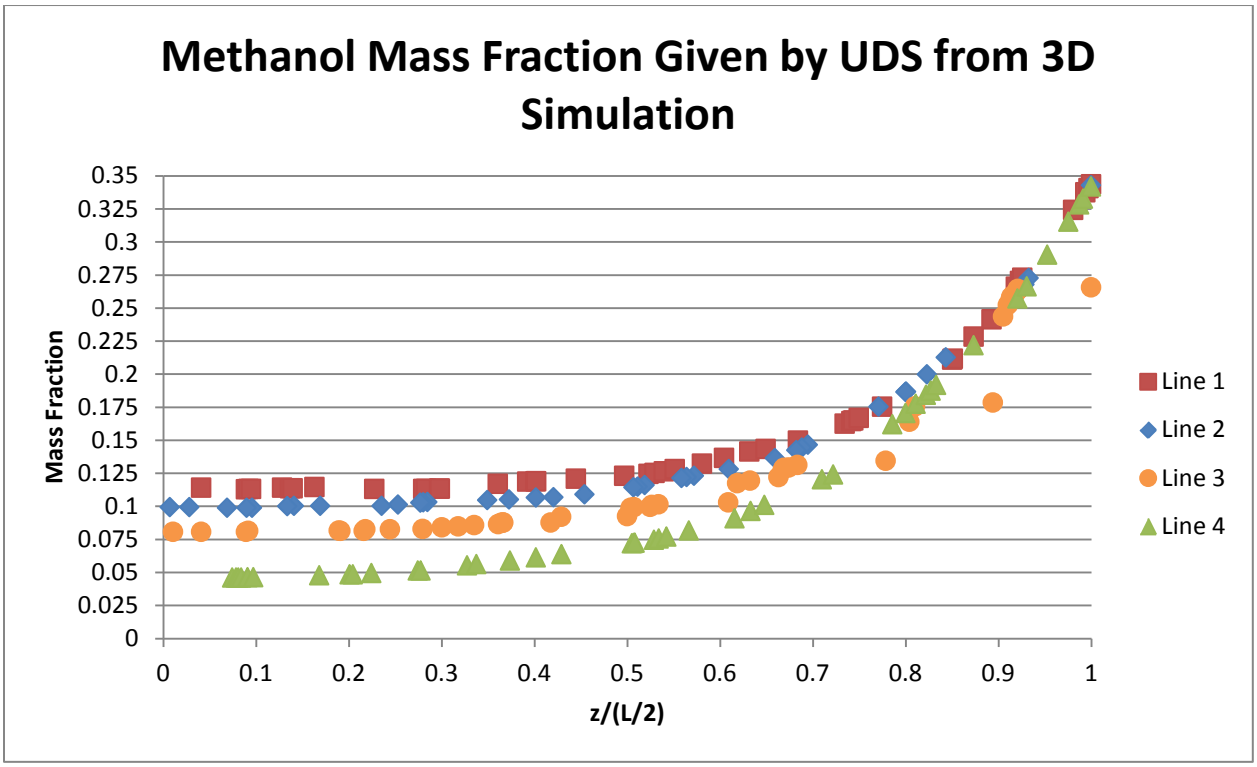

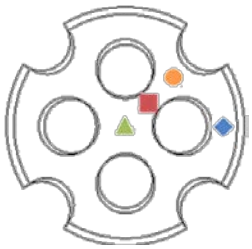

FIGURE 108: AXIAL PROFILE OF METHANOL MASS FRACTION AT FOUR SELECTED POINTS FOR 3D SIMULATION

of the length of the pellet, is presented in Figure 18. Additionally, Figure 18 presents data at four different locations within the 3D pellet, each of which exhibited different behavior due to the unique geometry of the catalyst. At each indicated point a line extends 0.005 m into the catalyst pellet, allowing for observation of methanol mass fraction. The radial profiles of methanol mass fraction resulting from all three 1D simulations provide a very good qualitative fit to the axial profile of methanol mass fraction given by the 3D simulation. In contrast to the results for overall reaction rate, the spherical pellet whose ratio of volume to surface area equals that of the pellet fits the data of the 3D simulation best. Although the molar flow rate of reactant into this sphere is lower than that of the other 1D models, the ratio of diffusion to reaction matches that of the 3D model much better.

The effect of the unique geometry of the 3D model is evident when considering the four selected regions for which methanol mass fraction is plotted in Figure 18. The region intersected by Line 1 has a much greater surface area to volume ratio than that of Line 4; therefore reactants can easily diffuse into that region to replace reactants consumed in the reaction, as evidenced by the higher mass fraction of methanol at this point. Similarly, Line 2 is closer to its nearest surfaces than Line 3, and an increased mass fraction of methanol was observed in this region. Line 4 intersects the center of the pellet, which shows the lowest methanol mass fraction due to the internal diffusion limitations which make it difficult for methanol to penetrate this region.

CHAPTER 6

Conclusions and Recommendations

The ability to simulate diffusion and reaction in catalytic systems offers great opportunities to investigate and optimize catalyst systems. Because of the complexity of three-dimensional models, it is desirable to approximate a three-dimensional model using a simpler one or two-dimensional equivalent. The reduction of a 3D model to a 1D or 2D model saves a considerable amount of time and effort when simulating a process for a variety of operating conditions.

The goal of this project was to simulate diffusion and reaction in a heterogeneous catalyst system in both a 3D and 1D model and evaluate whether the 1D model is a good approximation of the 3D model. The effect of the complex 3D geometry on diffusion and reaction was also characterized. Both the 3D and 1D models were verified by increasing the density of the mesh to see if any change in the simulation results was effected.

The 3D model showed good qualitative agreement with experimental H-NMR analysis of the same esterification reaction occurring over a catalyst pellet of the same geometry. Three 1D models were simulated, each using a different equivalent spherical radius. The overall reaction rates predicted by the 1D models were significantly lower than the overall reaction rate given by the 3D model. The best approximation of the overall reaction rate was given by the 1D model whose equivalent spherical radius was calculated by setting the surface area of the sphere equal to that of the 3D pellet; however this rate was only 32.68% of that given by the 3D model. All 1D models provided a good qualitative fit of the variation of methanol mass fraction with respect to relative radius. Furthermore, the 1D model whose ratio of surface area to volume equaled that of the 3D pellet provided an excellent quantitative fit of behavior at the center of the 3D catalyst pellet.

The current study could be immediately improved upon by utilizing a more complex approximation to the 3D model such as the generalized cylinder model (Mariani N. J., Keegan, Martinez,

& Barreto, 2003). Furthermore, the kinetic model employed in the simulation could be immediately improved upon by incorporating the mechanisms of adsorption into the rate law expression. Because the kinetic parameters presented in Chapter 3 do not account for these mechanisms values from literature for adsorption parameters would have to be used unless new kinetic experiments were devised.

NOMENCLATURE

a_v = catalyst surface area per reactor volume	$\left[\frac{1}{m}\right]$
A = pre-exponential factor	Varies
k_C = mass transfer coefficient	$\left[\frac{m}{s}\right]$
C_i = concentration of species i	$\left[\frac{kmol}{m^3}\right]$
C_{is} = concentration of species i on solid surface	$\left[\frac{kmol}{m^3}\right]$
c_P = heat capacity	$\left[\frac{J}{kg\ K}\right]$
D_e = effective diffusivity	$\left[\frac{m^2}{s}\right]$
D_{fluid} = fluid diffusivity	$\left[\frac{m^2}{s}\right]$
d_p = characteristic pellet diameter	[m]
d = diameter	[m]
E_a = activation energy	$\left[\frac{kJ}{mol}\right]$
H = enthalpy	[J]
h_f = heat transfer coefficient	$\left[\frac{W}{m^2K}\right]$
k = reaction rate constant	Varies
K = reaction equilibrium constant	$[-]$
k_{er} = effective thermal conductivity	$\left[\frac{W}{m\ K}\right]$
N = number of moles	[moles]
p = static pressure	[Pa]
r = radial coordinate	[m]
T = temperature	[K]

T_r = reference temperature	[K]
T_s= temperature on solid surface	[K]
t = time	[s]
u_s = superficial velocity	$\left[\frac{\mathrm{m}}{\mathrm{s}}\right]$
V = velocity	$\left[\frac{\mathrm{m}}{\mathrm{s}}\right]$
V = volume	$[\mathrm{m}^3]$
X = conversion	$\left[\frac{\text{moles reacted}}{\text{moles initial}}\right]$
x = coordinate	[m]
x_i = mole fraction of species i	$\left[\frac{\text{mol A}}{\text{mol}}\right]$
y = coordinate	[m]
Y_i = mass fraction of species i	$\left[\frac{\text{kg A}}{\text{kg}}\right]$
z = axial coordinate	[m]

Greek Letters

δ = boundary layer thickness	$[m]$
ε = bed voidage	$[-]$
μ = dynamic viscosity	$\left[\frac{kg}{m\ s}\right]$
η = effectiveness factor	$[-]$
ρ = density	$\left[\frac{kg}{m^3}\right]$

Dimensionless Flow Numbers

Re = Reynolds number	$[-]$
Sc = Schmidt number	$[-]$
Sh = Sherwood number	$[-]$

REFERENCES

Anderson, J. D. (1995). *Computational Fluid Dynamics: The Basics with Applications.* New York: McGraw-Hill, Inc.

Avci, A. K., Trimm, D. L., & Onsan, Z. I. (2001). Heterogeneous reactor modeling for simulation of catalytic oxidation and steam reforming of methane. *Chemical Engineering Science* , 641-649.

Dalman, M. T., Merkin, J. H., & McGreavy, C. (1986). Fluid flow and heat transfer past two spheres in a cylindrical tube. *Computers and Fluids* , 267-281.

Dixon, A. G., & Cresswell, D. L. (1987). Model Reduction for Two-Dimensional Catalyst Pellets with Complex Kinetics. *Industrial and Engineering Chemistry Research* , 2306-2312.

Dixon, A. G., Taskin, M. E., Nijemeisland, M., & Stitt, E. H. (2010). CFD Method to Couple Three-Dimensional Transport and Reaction inside Catalyst Particles to the Fixed Bed Flow Field. *Industrial and Engineering Chemistry Research* , 9012-9025.

DOW Ion Exchange Resins - Color Release. (2010, February 10). Retrieved 03 25, 2011, from DOW Answer Center: http://dow-answer.custhelp.com/app/answers/detail/a_id/4928/~/dow-ion-exchange-resins---color-release

du Toit, E., & Nicol, W. (2004). The rate inhibitine effect of water as a product on reactions catalysed by cation exchange resins: formation of mesityl oxide from aceton as case study. *Applied Catalysis* , 219-225.

Dyer, A. (2007). The Zeolite Scene - An Overview. In J. Cejka, H. van Bekkum, A. Corma, & F. Schuth, *Introduction to Zeolite Science and Practice* (pp. 525-554). Boston: Elsevier.

Fogler, H. S. (2006). *Elements of Chemical Reaction Engineering.* Boston: Prentice Hall.

Froment, G. F., & Bischoff, K. B. (1979). *Chemical Reactor Analysis and Design.* New York: John Wiley & Sons.

Harmer, M. A., & Sun, Q. (2001). Solid acid catalysts using ion-exchange resins. *Applied Catalysis* , 45-62.

Huang, J., Yijiao, J., Reddy Marthala, V. R., Wang, W., Sulikowski, B., & Hunger, M. (2007). In situ H MAS NMR investigations of the H/D exchange of alkylaromatic hydrocarbons on zeolites H-Y, La, Na-Y, and H-ZSM-5. *Microporous and Mesoporous Materials* , 86-90.

Industrial Catalysis. (n.d.). Retrieved March 20, 2011, from Johnson Matthey Catalysts: http://resources.schoolscience.co.uk/JohnsonMatthey/page14.htm

Maesen, T. (2007). The Zeolite Scene - An Overview. In J. Cejka, H. van Bekkum, A. Corma, & F. Schuth, *Introduction to Zeolite Science and Practice* (pp. 1-12). Boston: Elsevier.

Mariani, N. J., Keegan, S. D., Martinez, O. M., & Barreto, G. F. (2003). A One-Dimensional Equivalent Model to Evaluate Overall Reaction Rates in Catalytic Pellets. *Institution of Chemical Engineers* , 1033-1042.

Mariani, N. J., Keegan, S. D., Martinez, O. M., & Guillermo, F. B. (2008). On the evaluation of effective reaction rates on commercial catalyst by means of a one-dimensional modal. *Catalysis Today* , 770-774.

Nagaraj, A., & Mills, P. L. (2008). Analysis of Heat, Mass Transport, and Momentum Transport Effects in Complex Catalyst Shapes for Gas-Phase Heterogeneous Reactions Using Comsol Multiphysics. *COMSOL Conference 2008 Proceedings.* Boston.

Nijemeisland, M., & Dixon, A. G. (2001). Comparison of CFD simulations to experiment for convective heat transfer in a gas-solid fixed bed. *Chemical Engineering Journal* , 231-246.

Pedernera, M. N., Pina, J., Borio, D. O., & Bucala, V. (2003). Use of a heterogeneous two-dimensional model to improve the primary steam reformer performance. *Chemical Engineering Journal* , 29-40.

Popken, T., Gotze, L., & Gmehling, J. (2000). Reaction Kinetics and Chemical Equilibrium of Homogeneously and Heterogeneously Catalyzed Acetic Acid Esterification with Methanol and Methyl Acetate Hydrolysis. *Industrial and Engineering Chemistry Research* , 2601-2611.

Sie, S. T., & Kirshna, R. (1998). Process Development and Scale Up: II. Catalyst Design Strategy. *Reviews in Chemical Engineering* , 159-202.

Smith, J. M., Van Ness, H. C., & Abbott, M. M. (2005). *Introduction to Chemical Engineering Thermodynamics.* Boston: McGraw Hill.

Su, B.-L., & Norberg, V. (1997). Characterization of the Bronsted acid properties of H(Na)-Beta zeolite by infared spectroscopy and thermal analysis. *Zeolites* , 65-74.

Tannehill, J. C., Anderson, D. A., & Pletcher, R. H. (1997). *Computational Fluid Mechanics and Heat Transfer.* Washington, DC: Taylor & Francis.

Teo, H., & Saha, B. (2004). Heterogeneous catalysed esterification of acetic acid with isoamyl alcohol: kinetic studies. *Journal of Catalysis* , 174-182.

Zeiser, T., Lammers, P., Klemm, E., Li, Y. W., Bernsdorf, J., & Brenner, G. (2001). CFD-calculation of flow, dispersion, and reaction in a catalyst filled tube by the lattice Boltzmann method. *Chemical Engineering Science* , 1697-1704.

APPENDIX A

Gas-Liquid Chromatography Data Conversion

Tables A1 through A4 present each calculation in determining the pseudo-first order rate constant for each of the four experimental conditions described in Chapter 3. Table A5 presents each quantity used in determining the pseudo-homogeneous rate constant, activation energy, and pre-exponential factor. The variable x_i presents mole fraction data, the subscripts "AA" and "MA" refer to acetic acid and methyl acetate, respectively. The superscripts "exp.", "theory", and "crctd." refer to experimental, theoretical values, and corrected values, respectively.

Table A1: 40°C, 4 g Catalyst GLC Data Conversion

Time (s)	x_{AA}	x_{MA}	$x_{AA+MA}^{exp.}$	x_{AA+MA}^{theory}	$x_{AA}^{crctd.}$	$x_{MA}^{crctd.}$	Conversion (%)	$N_{reacted}$ (moles)	∂V (m^3)	V (m^3)	C_{AA} ($\frac{kmol}{m^3}$)	C_{MA} ($\frac{kmol}{m^3}$)	$\ln(C_{AA})$ ($\frac{kmol}{m^3}$)	$\ln(C_{MA})$ ($\frac{kmol}{m^3}$)
0	0.0000	0.0909	0.0909	0.07169	0.0000	0.1153	0.0000	0.0000	0.000E+00	2.100E-04	0.0000	2.6748	---	0.9839
1800	0.0081	0.0888	0.0969	0.07169	0.01027	0.1126	0.02310	0.1126	-3.058E-08	2.100E-04	0.2384	2.6134	-1.4339	0.9606
3600	0.0036	0.0876	0.0912	0.07169	0.00456	0.1111	0.03630	0.1769	-4.806E-08	2.100E-04	0.1060	2.5783	-2.2447	0.9471
5400	0.0135	0.0852	0.0987	0.07169	0.01712	0.1080	0.06271	0.3056	-8.301E-08	2.099E-04	0.3974	2.5081	-0.9228	0.9195
7200	0.0119	0.083	0.0949	0.07169	0.01509	0.1052	0.08691	0.4235	-1.150E-07	2.099E-04	0.3504	2.4437	-1.0488	0.8935
9000	0.015	0.0802	0.0952	0.07169	0.01902	0.1017	0.1177	0.5737	-1.558E-07	2.098E-04	0.4417	2.3617	-0.8171	0.8594
10800	0.0186	0.0788	0.0974	0.07169	0.02358	0.09992	0.1331	0.6487	-1.762E-07	2.098E-04	0.5478	2.3207	-0.6019	0.8419
12600	0.0209	0.0764	0.0973	0.07169	0.02650	0.09687	0.1595	0.7774	-2.112E-07	2.098E-04	0.6156	2.2504	-0.4851	0.8111
14400	0.0192	0.0756	0.0948	0.07169	0.02435	0.09586	0.1683	0.8203	-2.228E-07	2.098E-04	0.5656	2.2270	-0.5699	0.8006

Table A2: 50°C, 4 g Catalyst GLC Data Conversion

Time (s)	x_{AA}	x_{MA}	$x_{AA+MA}^{exp.}$	x_{AA+MA}^{theory}	$x_{AA}^{crctd.}$	$x_{MA}^{crctd.}$	Conversion (%)	$N_{reacted}$ (moles)	∂V (m^3)	V (m^3)	C_{AA} ($\frac{kmol}{m^3}$)	C_{MA} ($\frac{kmol}{m^3}$)	$\ln(C_{AA})$ ($\frac{kmol}{m^3}$)	$\ln(C_{MA})$ ($\frac{kmol}{m^3}$)
0	0	0.095	0.095	0.07169	0.00000	0.1259	0.0000	0.0000	0.0000	2.100E-04	0.0000	2.922		1.072
1800	0.0087	0.1055	0.1142	0.07169	0.01153	0.1398	0.1105	0.5386	-1.463E-07	2.099E-04	0.2677	3.247	-1.318	1.178
3600	0.018	0.0981	0.1161	0.07169	0.02385	0.1300	0.03263	0.1590	-4.320E-08	2.100E-04	0.5537	3.017	-0.5912	1.104
5400	0.0227	0.0918	0.1145	0.07169	0.03008	0.1217	0.03368	0.1642	-4.459E-08	2.100E-04	0.6982	2.824	-0.3592	1.038
7200	0.0257	0.0885	0.1142	0.07169	0.03406	0.1173	0.06842	0.3334	-9.057E-08	2.099E-04	0.7907	2.723	-0.2348	1.002
9000	0.0337	0.0854	0.1191	0.07169	0.04466	0.1132	0.1011	0.4925	-1.338E-07	2.099E-04	1.037	2.628	0.03637	0.9662
10800	0.0272	0.0871	0.1143	0.07169	0.03605	0.1154	0.08316	0.4053	-1.101E-07	2.099E-04	0.8369	2.680	-0.1780	0.9858
12600	0.0415	0.0774	0.1189	0.07169	0.05500	0.1026	0.1853	0.9029	-2.452E-07	2.098E-04	1.278	2.383	0.2451	0.8684
14400	0.0469	0.074	0.1209	0.07169	0.06215	0.09806	0.2211	1.077	-2.926E-07	2.097E-04	1.444	2.279	0.3676	0.8237

Table A3: 60°C, 4 g Catalyst GLC Data Conversion

Time (s)	x_{AA}	x_{MA}	$x_{AA+MA}^{exp.}$	x_{AA+MA}^{theory}	$x_{AA}^{crctd.}$	$x_{MA}^{crctd.}$	Conversion (%)	$N_{reacted}$ (moles)	∂V (m^3)	V (m^3)	C_{AA} ($\frac{kmol}{m^3}$)	C_{MA} ($\frac{kmol}{m^3}$)	$\ln(C_{AA})$ ($\frac{kmol}{m^3}$)	$\ln(C_{MA})$ ($\frac{kmol}{m^3}$)
0	0.0000	0.095	0.095	0.07169	0.00000	0.1259	0.0000	0.0000	0.0000	2.100E-04	0.0000	2.922	----	1.072
1800	0.025	0.0788	0.1038	0.07169	0.03313	0.1044	0.1705	0.8310	-2.257E-07	2.098E-04	0.7697	2.426	-0.2618	0.8862
3600	0.0124	0.081	0.0934	0.07169	0.01643	0.1073	0.1474	0.7182	-1.951E-07	2.098E-04	0.3817	2.493	-0.9631	0.9136
5400	0.0387	0.0719	0.1106	0.07169	0.05128	0.09528	0.2432	1.185	-3.219E-07	2.097E-04	1.192	2.215	0.1756	0.7950
7200	0.0499	0.067	0.1169	0.07169	0.06613	0.08879	0.2947	1.436	-3.902E-07	2.096E-04	1.537	2.064	0.4301	0.7248
9000	0.0561	0.0605	0.1166	0.07169	0.07434	0.08017	0.3632	1.770	-4.807E-07	2.095E-04	1.729	1.865	0.5477	0.6232
10800	0.0684	0.0549	0.1233	0.07169	0.09064	0.07275	0.4221	2.057	-5.588E-07	2.094E-04	2.109	1.693	0.7463	0.5264
12600	0.0635	0.0515	0.115	0.07169	0.08415	0.06825	0.4579	2.231	-6.061E-07	2.094E-04	1.958	1.588	0.6722	0.4627

Table A4: 60°C, 8 g Catalyst GLC Data Conversion

Time (s)	x_{AA}	x_{MA}	$x_{AA+MA}^{exp.}$	x_{AA+MA}^{theory}	$x_{AA}^{crctd.}$	$x_{MA}^{crctd.}$	Conversion (%)	$N_{reacted}$ (moles)	∂V (m^3)	V (m^3)	C_{AA} ($\frac{kmol}{m^3}$)	C_{MA} ($\frac{kmol}{m^3}$)	$\ln(C_{AA})$ ($\frac{kmol}{m^3}$)	$\ln(C_{MA})$ ($\frac{kmol}{m^3}$)
0	0.0000	0.095	0.095	0.07169	0.0000	0.1259	0.0000	0.0000	0.0000	2.100E-04	0.00000	2.922	---	1.072
1800	0.0458	0.079	0.1248	0.07169	0.06069	0.1047	0.1684	0.8208	-2.229E-07	2.098E-04	1.410	2.432	0.3436	0.8887
3600	0.0691	0.0652	0.1343	0.07169	0.09157	0.08640	0.3137	1.529	-4.152E-07	2.096E-04	2.129	2.009	0.7558	0.6977
5400	0.0901	0.0524	0.1425	0.07169	0.1194	0.06944	0.4484	2.185	-5.936E-07	2.094E-04	2.779	1.616	1.022	0.4800
7200	0.0995	0.0421	0.1416	0.07169	0.1319	0.05579	0.5568	2.714	-7.371E-07	2.093E-04	3.071	1.299	1.122	0.2618
9000	0.1057	0.0341	0.1398	0.07169	0.1401	0.04519	0.6411	3.124	-8.486E-07	2.092E-04	3.264	1.053	1.183	0.05158
10800	0.124	0.0292	0.1532	0.07169	0.1643	0.03870	0.6926	3.375	-9.169E-07	2.091E-04	3.830	0.9019	1.343	-0.1032

TABLE A5: QUANTITIES USED TO CALCULATE KINETIC PARAMETERS

T (s)	$m_{catalyst}$ (g)	k' (s^{-1})	k' ($\frac{m^3}{s\ kg_{catalyst}}$)	k ($\frac{m^6}{s\ kmolkg_{catalyst}}$)	A ($\frac{m^6}{s\ kmolkg_{catalyst}}$)
313.15	4	$1.345*10^{-5}$	$7.060*10^{-7}$	$3.335*10^{-8}$	-17.22
323.15	4	$2.065*10^{-5}$	$1.084*10^{-6}$	$5.121*10^{-8}$	-16.79
333.15	4	$4.634*10^{-5}$	$2.433*10^{-6}$	$1.148*10^{-7}$	-15.98
333.15	8	$1.118*10^{-4}$	$2.935*10^{-6}$	$2.494*10^{-7}$	-15.20

APPENDIX B

Sample Gambit Journal

```
/ Journal File for GAMBIT 2.4.6, Database 2.4.4, ntx86 SP2007051421
/ Identifier "default_id3100"
/ File opened for write Thu Jan 13 19:40:29 2011.
identifier name "Catalyst System" new nosaveprevious
volume create height 0.01 radius1 0.0175 radius2 0.0175 radius3 0.0175 offset \
  0 0 0.005 zaxis frustum
volume create height 0.01 radius1 0.00425 radius2 0.00425 radius3 0.00425 \
  offset 0 0 0.005 zaxis frustum
volume move "volume.2" offset -0.0085 0 0
volume cmove "volume.2" multiple 1 offset 0.017 0 0
volume cmove "volume.3" multiple 1 offset -0.0085 0.0085 0
volume cmove "volume.3" multiple 1 offset -0.0085 -0.0085 0
volume cmove "volume.3" multiple 1 offset -0.0085 0 0
volume cmove "volume.6" multiple 1 offset 0.012374 0.012374 0
volume cmove "volume.6" multiple 1 offset -0.012374 0.012374 0
volume cmove "volume.6" multiple 1 offset 0.012374 -0.012374 0
volume move "volume.6" offset -0.012374 -0.012374 0
volume subtract "volume.1" volumes "volume.8" "volume.4" "volume.7" \
  "volume.3" "volume.9" "volume.5" "volume.2" "volume.6"
```

```
volume create height 0.27 radius1 0.02 radius2 0.02 radius3 0.02 offset 0 0 \
  0.135 zaxis frustum
volume move "volume.1" offset 0 0 0.07
volume subtract "volume.2" volumes "volume.1" keeptool
face modify "face.7" label "PELLET HOLE (X)"
face modify "face.10" label "PELLET HOLE (Y)"
face modify "face.5" label "PELLET HOLE (-X)"
face modify "face.13" label "PELLET HOLE (-Y)"
face modify "face.29" label "PELLET FACE (-Z)"
face modify "face.34" label "PELLET FACE (Z)"
face modify "face.2" label "PELLET WALL (Y)"
face modify "face.31" label "PELLET WALL (X)"
face modify "face.30" label "PELLET WALL (-X)"
face modify "face.33" label "PELLET WALL (-Y)"
face modify "face.19" label "PELLET WALL (I)"
face modify "face.25" label "PELLET WALL (IV)"
face modify "face.16" label "PELLET WALL (III)"
face modify "face.22" label "PELLET WALL (II)"
face modify "face.45" label "REACTOR HOLE (X)"
face modify "face.47" label "REACTOR FACE (-Z)"
face modify "face.49" label "REACTOR HOLE (Y)"
face modify "face.41" label "REACTOR HOLE (-X)"
face modify "face.42" label "REACTOR HOLE (-Y)"
face modify "face.39" label "REACTOR FACE (Z)"
face modify "face.51" label "REACTOR WALL (Y)"
face modify "face.44" label "REACTOR WALL (X)"
```

```
face modify "face.40" label "REACTOR WALL (-Y)"
face modify "face.48" label "REACTOR WALL (-X)"
face modify "face.46" label "REACTOR WALL (I)"
face modify "face.43" label "REACTOR WALL (IV)"
face modify "face.38" label "REACTOR WALL (III)"
face modify "face.50" label "REACTOR WALL (II)"
face modify "face.35" label "VELOCITY INLET"
face modify "face.36" label "TUBE WALL"
face modify "face.37" label "PRESSURE OUTLET"
face connect "PELLET HOLE (-X)" "REACTOR HOLE (-X)" real
face connect "PELLET WALL (Y)" "REACTOR WALL (Y)" real
face connect "PELLET HOLE (X)" "REACTOR HOLE (X)" real
face connect "PELLET HOLE (Y)" "REACTOR HOLE (Y)" real
face connect "PELLET HOLE (-Y)" "REACTOR HOLE (-Y)" real
face connect "PELLET WALL (I)" "REACTOR WALL (I)" real
face connect "PELLET WALL (II)" "REACTOR WALL (II)" real
face connect "PELLET WALL (III)" "REACTOR WALL (III)" real
face connect "PELLET WALL (IV)" "REACTOR WALL (IV)" real
face connect "PELLET WALL (-X)" "REACTOR WALL (-X)" real
face connect "PELLET WALL (X)" "REACTOR WALL (X)" real
face connect "PELLET FACE (-Z)" "REACTOR FACE (-Z)" real
face connect "PELLET FACE (Z)" "REACTOR FACE (Z)" real
face connect "PELLET WALL (-Y)" "REACTOR WALL (-Y)" real
physics create "WALL" btype "WALL" face "TUBE WALL"
physics create "PELLET" btype "WALL" face "TUBE WALL" "PELLET WALL (Y)" \
  "PELLET HOLE (-X)" "PELLET HOLE (X)" "PELLET HOLE (Y)" "PELLET HOLE (-Y)" \
```

```
  "PELLET WALL (III)" "PELLET WALL (I)" "PELLET WALL (II)" "PELLET WALL (IV)" \
  "PELLET FACE (-Z)" "PELLET WALL (-X)" "PELLET WALL (X)" "PELLET WALL (-Y)" \
  "PELLET FACE (Z)"
physics create btype "VELOCITY_INLET" face "VELOCITY INLET"
physics create "PRESSURE O+UTLET" btype "PRESSURE_OUTLET" face \
  "PRESSURE OUTLET"
physics modify "velocity_inlet.2" btype label "VELOCITY INLET" face \
  "VELOCITY INLET"
face mesh "PELLET WALL (Y)" "PELLET HOLE (-X)" "PELLET HOLE (X)" \
  "PELLET HOLE (Y)" "PELLET HOLE (-Y)" "PELLET WALL (III)" "PELLET WALL (I)" \
  "PELLET WALL (II)" "PELLET WALL (IV)" "PELLET FACE (-Z)" "PELLET WALL (-X)" \
  "PELLET WALL (X)" "PELLET WALL (-Y)" "PELLET FACE (Z)" triangle size \
  0.0005
volume mesh "volume.2" tetrahedral size 0.01
volume mesh "volume.1" tetrahedral size 0.001
physics create "FLUID" ctype "FLUID" volume "volume.2"
physics create "SOLID" ctype "SOLID" volume "volume.1"
save
export fluent5 "Catalyst System.msh"
```

APPENDIX C

3D Simulation Convergence Plots

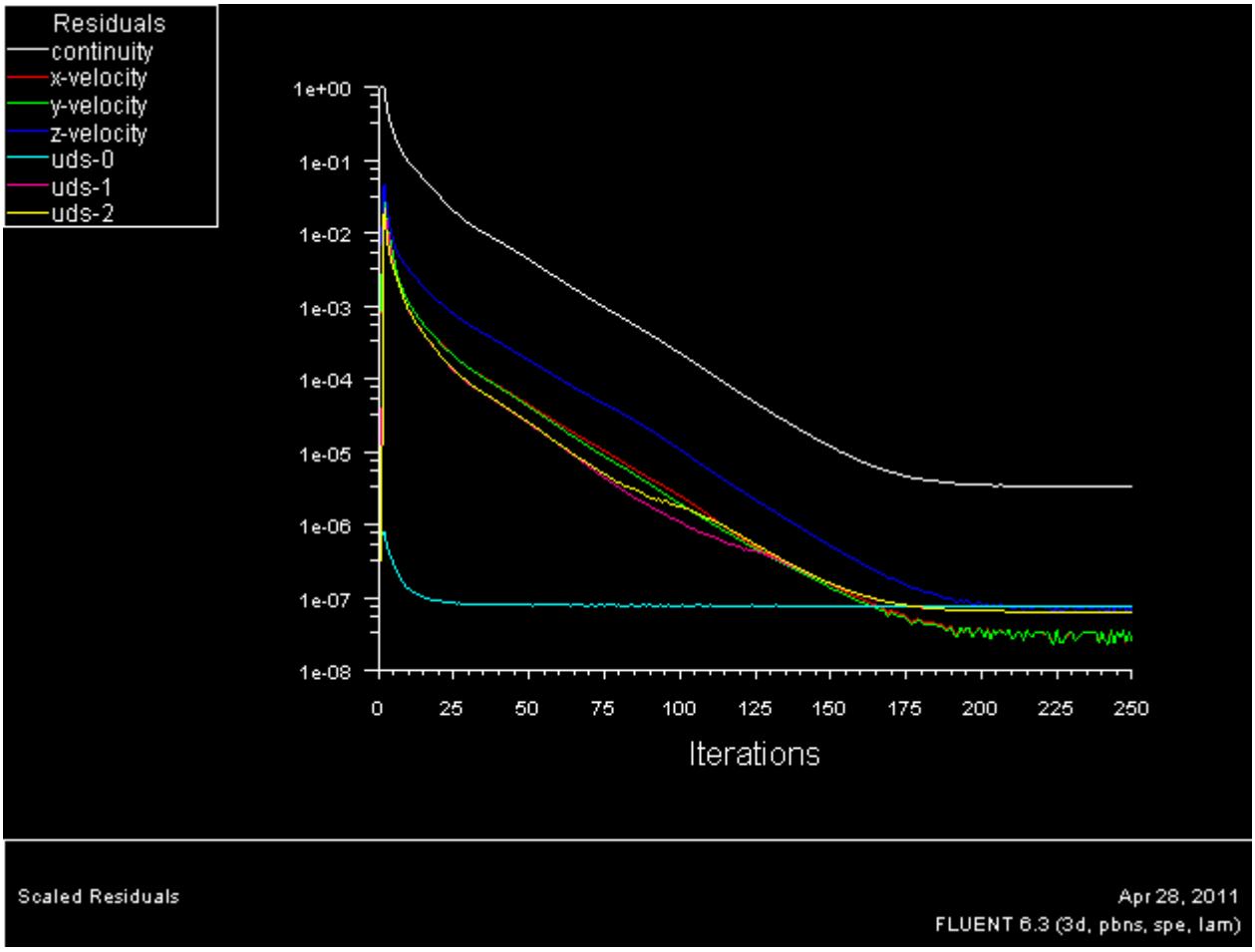

FIGURE 1911: UNREFINED MESH CONVERGENCE PLOT

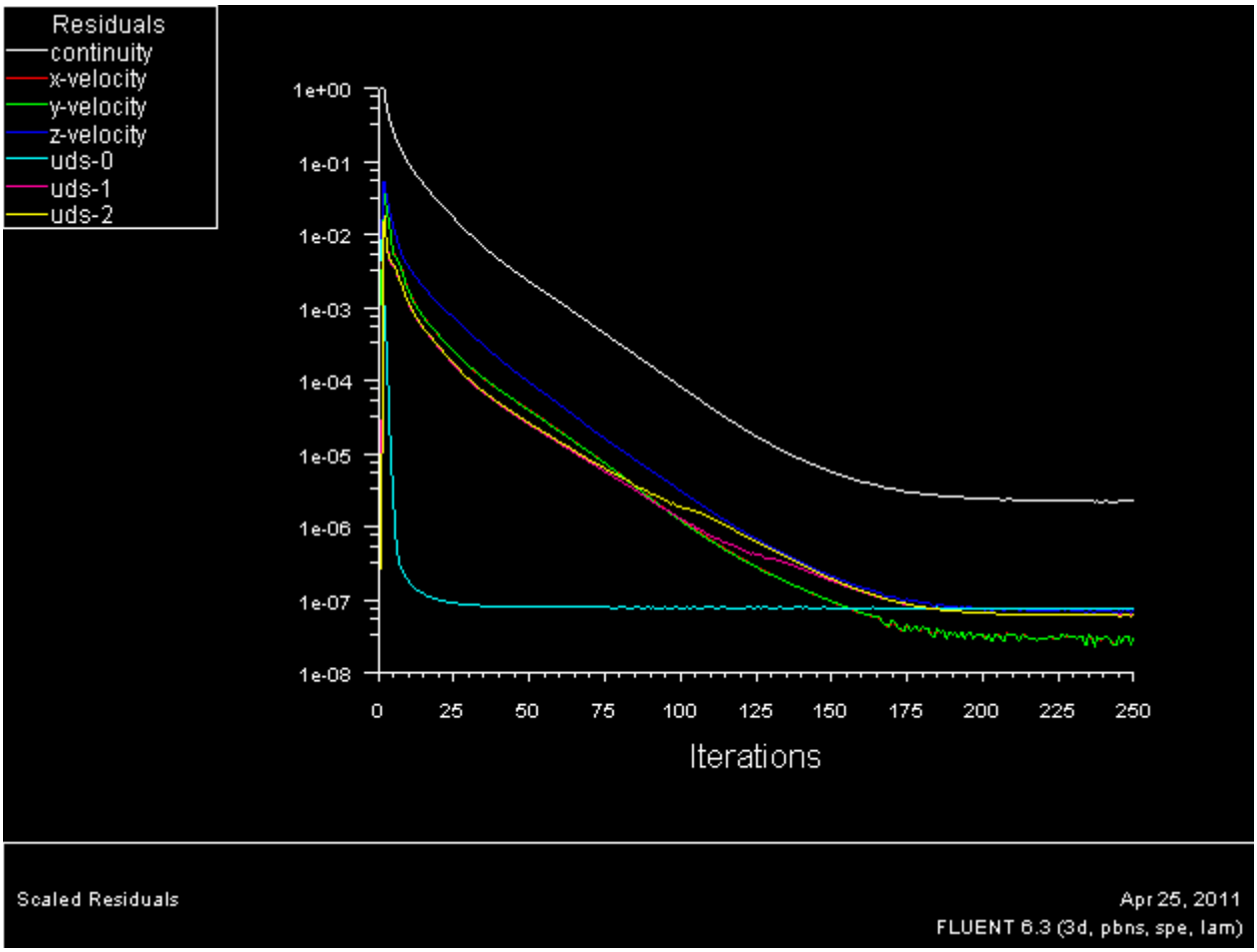

FIGURE 120: REFINED MESH CONVERGENCE PLOT